Physics Letters A 444 (2022) 128226

Contents lists available at ScienceDirect

Physics Letters A

www.elsevier.com/locate/pla

Enhanced s^*-wave component of the superconducting gap in overdoped HTSC cuprates with orthorhombic distortion

I.A. Makarov *, S.G. Ovchinnikov

Kirensky Institute of Physics, Federal Research Center KSC SB RAS, Akademgorodok 50, bld. 38, 660036 Krasnoyarsk, Russia

ARTICLE INFO

Article history:
Received 16 January 2022
Received in revised form 24 April 2022
Accepted 21 May 2022
Available online 24 May 2022
Communicated by L. Ghivelder

Keywords:
High-Tc superconductors
Orthorhombic cuprates
Hubbard model
Superconductivity theory
Fermi contour
Superconducting gap symmetry

ABSTRACT

In this work, the concentration and temperature dependence of the superconducting gap of the HTSC cuprate in the orthorhombic phase are obtained within the framework of the Hubbard model taking into account the exchange mechanism of pairing. To elucidate the reasons for the unexpectedly large s^*-wave component of the superconducting gap in the overdoped regime, the electronic structure of low-energy excitations and the **k**-dependent contributions of pair states to the gap components were investigated. It is shown that the s^*-wave component growth results from the shallowing of the electron pocket in the region of the s^*-wave component maximum.

1. Introduction

The mechanism of superconducting pairing in HTSC cuprates is still a subject of discussion. The symmetry and magnitude of the superconducting gap are important characteristics that can indicate an active pairing mechanism. It is generally accepted that the superconducting gap in HTSC cuprates has d-wave symmetry since a large number of experimental data of different types jointly support this type of symmetry. The heat capacity [1–4], penetration depth [5–7], and thermal conductivity [8–10] experiments indicate the presence of superconducting gap nodes. ARPES experiments, which can provide direct information on the momentum dependence of the superconducting gap, have shown that the superconducting gap in cuprates is highly anisotropic and close to zero in the nodal direction [11–14]. Phase-sensitive experiments have demonstrated a π phase shift of the order parameter between the orthogonal directions a and b in $YBa_2Cu_3O_{7-\delta}$ (YBCO) [15–19] and the half-integer flux quantum effect in YBCO [20,21], $Tl_2Ba_2CuO_{4+\delta}$ [22] and $Bi_2Sr_2CaCu_2O_8$ (Bi2212) [23]. All these experimental data agree with the results that should be observed for the d-wave gap. However, these data also do not exclude a small admixture of components of different symmetry, since the error and insufficient resolution do not allow to make an unambiguous conclusion that the superconducting gap in cuprates has a pure d-wave symmetry. For example, the ARPES studies [11,12] directly admit the impossibility of distinguishing whether the superconducting gap in the nodal direction is zero or has a small but finite value. It is also necessary to bear in mind the sensitivity of experimental techniques to the surface and volume of the sample since the shape of the superconducting gap can differ at different depths in the sample [24]. But the most important factors that can affect the symmetry of the superconducting gap are the crystal lattice structure and doping of the sample under study.

Among cuprates, there are compounds with both tetragonal and orthorhombic crystal lattice structures. Since it is believed that the superconductivity is formed in CuO_2 layers, the superconducting gap symmetry should reflect the symmetry of the CuO_2 lattice. This means that real tetragonal and orthorhombic structures are reduced simply to square and rectangular lattices. The form of the superconducting gap in position and momentum space refers to one of the irreducible representations of the symmetry group of the crystal lattice. The square lattice has four irreducible representations: A_{1g}, A_{2g}, B_{1g}, B_{2g}. The corresponding states with singlet pairing are designated as $s+$, g, $d_{x^2-y^2}$, d_{xy} [25,26]. In a rectangular lattice, the pair states $s+$ and $d_{x^2-y^2}$ belong to the same irreducible representation A_{1g}, and the superconducting gap is a mixture of d-wave and s-wave gap functions [27,28]. The superconducting gap cannot have pure d-wave

* Corresponding author.
E-mail addresses: maki@iph.krasn.ru (I.A. Makarov), sgo@iph.krasn.ru (S.G. Ovchinnikov).

https://doi.org/10.1016/j.physleta.2022.128226
0375-9601/

symmetry in orthorhombic samples, although the s-wave component is apparently very small since it does not manifest itself clearly in the nodal direction in ARPES experiments near optimal doping.

The momentum dependence of the superconducting gap reflects not just the **k**-dependence of the pairing interaction, but also the joint **k**-dependence of the energy and spectral weight of electronic states. Doping significantly reconstructs the electronic structure of cuprates. Doping of the parent compound in the state of an antiferromagnetic insulator leads to the destruction of the long-range magnetic order, but the short-range magnetic order is preserved. An unusual pseudogap electronic state appears in the region of weak and optimal doping. As the doping increases, the direction in **k**-space along which the pseudogap closes changes from nodal to antinodal. The pseudogap disappears over the entire Fermi surface at the concentration of doped holes p^*, and the electrons begin to behave like a normal paramagnetic Fermi liquid, while the superconducting phase still exists.

Since the electronic structure of cuprates changes significantly with doping, it is expected that the **k**-dependence of the superconducting gap will also change depending on the number of charge carriers even if the pairing interaction does not depend on the carrier concentration. Indeed, it was shown in [29] that the degree of the superconducting gap anisotropy changes with increasing doping. Comparison between the ARPES spectra in underdoped and overdoped Bi2212 samples demonstrates a significant increase in the superconducting gap along the nodal direction with oxygen doping and the absence of pure d-wave symmetry of the gap in the overdoped composition [29]. The change in the size of the superconducting gap along the nodal direction with doping was detected using ARPES in slightly and heavily overdoped Bi2212 [30]. While in a slightly overdoped cuprate the superconducting gap in the nodal direction has a small value that can be considered zero of the d-wave order parameter, the nodal gap is significant in a heavily overdoped compound and cannot be considered zero. The results of these and other experiments can be interpreted in terms of a two-component order parameter. The theoretical works [31–33] confirm the conclusion about the presence of the two-component order parameter in cuprates.

The ARPES experiment on overdoped YBCO [34] showed a difference in the superconducting gap magnitude and the superconducting peak intensity between measurements along the x and y axes. These features indicate a deviation from the d-wave gap function. Raman scattering spectra also demonstrate an $x-y$ difference [35]. The energies of the pair-breaking peaks of the imaginary part of the electronic response function in the xx and yy polarizations and the widths of these peaks are different in YBCO. These features are most pronounced in overdoped compounds, although are also observed in underdoped and optimally doped samples. The position of the pair-breaking peak in the Raman spectra serves as an indicator of the superconducting gap size. A change in the relative position of the pair-breaking peaks in the Raman spectra of different polarizations may indicate a change in the symmetry of the superconducting gap. The specific features of the overdoping effect on the Raman spectra in cuprates are a decrease in the energies of the pair-breaking peaks, a change in the ratio of these energies in the spectra of different symmetry, and a change in the intensity of the pair-breaking peaks, which has a different character for the spectra of different symmetry [36–42]. Raman spectra in optimally doped and overdoped cuprates YBCO, Bi2212, and Hg1212 were explained in [40] by considering the $d+s$ symmetry of the superconducting gap.

The dependence of tunneling conductance on voltage in scanning tunneling spectroscopy in underdoped and optimally doped samples of Ca-doped YBCO [43] is consistent with theories based on the d-wave symmetry of the superconducting gap. However, the presence of symmetric subgap peaks in overdoped samples indicates doping-induced changes in the pairing symmetry [43]. The spectra of the overdoped Ca-doped YBCO were described using the generalized Blonder, Tinkham and Klapwijk (BTK) theory with $d+s$ pairing symmetry [43].

Evidences for the presence of the s-wave component of the superconducting gap in orthorhombic cuprates were obtained in Josephson tunneling studies [44,45] and in measurements of the $a-b$ anisotropy of the penetration depth in spectroscopic measurements in the microwave and far-infrared ranges [46,47]. The superconducting gap with d- and s-wave components was found in measurements of thermal conductivity in YBCO [10].

Theoretical studies also demonstrate the mixing of s^*-wave symmetry with the d-wave superconducting gap in the orthorhombic phase of cuprates. A large fraction of the s^*-wave component in the superconducting gap was obtained in [48] within the framework of the $t-J$ model, but its concentration dependence was not discussed. The dependence of the ratio of the d- and s^*-wave components of the superconducting gap on the chemical potential level was found in [49]. The change in this ratio is the main result of doping within the rigid-band model, but the joint change in the electronic structure and the ratio of components with doping has not been studied.

It can be seen from the above experimental data that the s-wave component is admixed to the d-wave component of the superconducting gap in overdoped cuprates. At least two possible reasons for this behavior with doping can be indicated: a change in the pairing mechanism, or a change in the electronic structure. Since it is known that a change in the concentration of charge carriers from the optimally doped to the overdoped regime in cuprates leads to the transformation of the electron system from the pseudogap state to the normal Fermi liquid, the second possibility seems more realistic. In this work, we theoretically investigate the dependence of the superconducting gap on doping and temperature and try to understand the mechanism of the change in the ratio of the components of the superconducting gap upon doping. The theory of BCS-type superconductivity is constructed within the framework of the Hubbard model for excitations in a planar rectangular lattice of CuO_6 octahedra, which simulates the HTSC cuprate $La_{2-x}Sr_xCuO_4$. A system of equations for the d- and extended s^*-wave components of the superconducting gap is obtained taking into account the anisotropic exchange mechanism of pairing. The self-consistent solution of this system determines the superconducting gap at various values of doping, temperature, and pairing constants. A significant change in the ratio of the d- and s^*-wave components with doping was found within this approach. The dispersion surface and the Fermi contour were calculated in order to determine the structure of the electronic states that are involved in the pairing. Further analysis of the **k**-dependent contributions of these states to the components of the superconducting gap allowed to find out which pair states are responsible for the observed features of the concentration dependence of the superconducting gap.

The paper includes four sections. Section 2 describes the Hamiltonian of the Hubbard model for excitations in a rectangular lattice and reports the method we used to calculate the superconducting gap. In Section 3, we present and discuss the results of a study of the superconducting gap symmetry in orthorhombic cuprates and the reasons for its unusual behavior. Subsection 3.1 is devoted to the concentration and temperature dependences of the d- and s^*-wave components of the superconducting gap. Subsection 3.2 reports on the electronic structure of low-energy excitations in the normal and superconducting phase and their transformation with doping in the overdoped regime. In subsection 3.3, we analyze the contributions of electronic states with different wave vectors to the d- and s^*-wave components of the superconducting gap. In subsection 3.4, we discuss the factors that can reduce the s^*-wave component in real compounds. Section 4 summarizes the main results.

2. Theoretical model and calculation method. Superconducting state in the Hubbard model with the *d*- and extended *s**-wave components of the superconducting gap

There is a large number of theoretical papers devoted to superconductivity in the Hubbard model in a 2D square lattice, see recent reviews [50,51] and a few papers concerning the orthorhombic phase. The influence of orthorhombic distortion on the band structure, density of states, Fermi contour, and the concentration dependence of T_c in a wide range of hole doping (from $x = 0$ to 0.3) in HTSC cuprates was studied in [52]. In this paper, we investigate the concentration and temperature dependences of the components of the superconducting gap, i.e. symmetry of the superconducting gap, at a fixed orthorhombic distortion, and elucidate the origin of the unusual feature found in the concentration dependence. The elucidation of the reasons for the unusual behavior required the calculation of the band structure and the Fermi surface specifically at those concentrations in the overdoped regime at which the unusual behavior is observed. In addition to the band structure, we plot spectral functions convenient for comparison with the ARPES data. We calculated the dependence of the modulus of the superconducting gap on the wave vector, and this allowed us to conclude that the symmetry of the superconducting gap differs in different regions of the Brillouin zone. Besides, the distribution of contributions to the components of the superconducting gap of different symmetry in the momentum space is used here for the first time as a tool for analyzing the change in the ratio of these components with doping.

We will study the symmetry properties of the superconducting gap in cuprates using the example of a mono-layer p-type compound $La_{2-x}Sr_xCuO_4$. We model this compound by a layer of CuO_6 octahedra, assuming that the remaining structural elements are responsible only for the supply of charges to this layer. To describe the electronic structure, we start with a five-band p-d model for holes in the CuO_6 layer of octahedra, this model includes copper $d_{x^2-y^2}$, $d_{3z^2-r^2}$ orbitals, p_x,p_y planar oxygen orbitals, and a bonding p_z orbital of apical oxygens. In order to correctly take into account strong electron correlations, the generalized tight-binding (GTB) method [53–55] was used. This method is a cluster perturbation theory in the language of Hubbard operators. In this method, the crystal lattice is divided into clusters, the total Hamiltonian is written as the sum of the Hamiltonian of intracluster interactions and the Hamiltonian of interactions of particles from different clusters. The many-body cluster eigenstates are calculated using exact diagonalization. In the orthorhombic phase, the multiparticle cluster eigenstates are a mixture of all five orbitals of the p-d model. Fermi-type excitations between the obtained multiparticle states form a new basis of quasiparticles of the multiband Hubbard model, each of the new excitations is described by the Hubbard operator. These quasiparticle excitations are called the Hubbard fermions. At the last stage of the GTB method, the full Hamiltonian is written in terms of new quasiparticle excitations. The total Hilbert space of the unit cell in this approach is very large and includes all ground and excited states for different hole numbers $n = 0, 1, 2, 3$ etc. per CuO_6 cluster. Nevertheless in the low-energy limit the number of essential states is not large. The undoped cuprate contains one hole in the mixed Cu d- and O p-molecular orbital, with spin 1/2 two-fold degeneracy. The electron addition results in the hole vacuum state with $n = 0$. The electron removal due to hole doping results in the two-hole term that is a linear combination of the Zhang-Rice singlet with a hole on Cu and a hole on O, as well as two holes at different O ions. Formally, the low-energy minimal number of states corresponds to the Hubbard model local eigenstates, that is why the Hubbard model is the effective low-energy model to study the low-energy electronic states and properties of cuprates.

Cluster eigenstates that participate in the formation of the Hubbard model basis are the ground state of a cluster with zero holes $|0\rangle$, the spin doublet of the ground one-hole state $|\sigma\rangle$ with $\sigma = \pm 1/2$, the ground two-hole singlet state $|S\rangle$. Excitations between zero-hole and one-hole states (0σ), $(0\bar{\sigma})$ form the upper Hubbard band of the correlated electrons, excitations between one-hole and two-hole states (σS), $(\bar{\sigma} S)$ form the lower Hubbard band. Each quasiparticle excitation (pq) is determined by two indices p and q, denoting the initial and final cluster eigenstates, between which the transition occurs. We can order the four Fermi-type quasiparticles in the basis of Hubbard model as follows: $\{(0\bar{\sigma}), (\sigma S), (0\sigma), (\bar{\sigma} S)\}$. And we can perform a one-to-one correspondence between this series and another set of elements that consists of the serial numbers of the corresponding elements of the double-index series: 1, 2, 3, 4. The elements of the new series are the values of single index α, which now also characterizes each quasiparticle excitation. Since the bands of quasiparticles with opposite spin projections are degenerate in energy, below we will deal with two quasiparticles $(0\bar{\sigma}), (\sigma S)$ with spin projection $-1/2$. The single-index notation α includes two values, 1 and 2, which characterize the upper and lower Hubbard subbands, respectively. That is, there are two types of designation of quasiparticle excitations. In what follows, both notations will be used.

The Hamiltonian of the Hubbard model in terms of the Hubbard X-operators is given by the expression:

$$H = \sum_f \varepsilon_0 X_f^{00} + \sum_{f\sigma} (\varepsilon_\sigma - \mu) X_f^{\sigma\sigma} + \sum_f (\varepsilon_S - 2\mu) X_f^{SS} + \sum_{fg\sigma} \sum_{pqmn} t_{fg\sigma}(pq, mn) X_f^{pq} X_g^{mn}, \tag{1}$$

where ε_0, ε_σ, ε_S are the energies of the states $|0\rangle$, $|\sigma\rangle$, $|S\rangle$, respectively, μ is the chemical potential. $t_{fg\sigma}(pq, mn)$ are the hopping integrals between the quasiparticle excitations (pq) and (mn) in the sites f and g, respectively. We will consider only one value of the orthorhombicity factor for the lattice of CuO_6 octahedra: $(b - a)/a = 4.15\%$, where a, b are the lattice parameters. We take the numerical values of the Hamiltonian parameters ε_0, ε_σ, ε_S, $t_{fg\sigma}(pq, mn)$ from [52].

In this work, to obtain the spectrum of quasiparticles and the superconducting gap in an HTSC cuprate with orthorhombic distortion, we use the same technique that was used in [56] to describe its tetragonal phase. The quasiparticle spectrum and the superconducting gap were obtained using the equation of motion method for a Green's function. The Green's function, constructed on excitations $\{(0\bar{\sigma}), (\sigma S), (\sigma 0), (S\bar{\sigma})\}$, corresponding to electron removal and electron addition excitations in the basis of Hubbard model, is the 4×4 matrix (which consists of the 2×2 matrices of the normal and anomalous components):

$$\hat{D}^{\bar{\sigma}}(f, g) = \begin{bmatrix} \left\langle\left\langle X_f^{0\bar{\sigma}} \middle| X_g^{\bar{\sigma}0}\right\rangle\right\rangle & \left\langle\left\langle X_f^{0\bar{\sigma}} \middle| X_g^{S\sigma}\right\rangle\right\rangle & \left\langle\left\langle X_f^{0\bar{\sigma}} \middle| X_g^{0\sigma}\right\rangle\right\rangle & \left\langle\left\langle X_f^{0\bar{\sigma}} \middle| X_g^{\bar{\sigma}S}\right\rangle\right\rangle \\ \left\langle\left\langle X_f^{\sigma S} \middle| X_g^{\bar{\sigma}0}\right\rangle\right\rangle & \left\langle\left\langle X_f^{\sigma S} \middle| X_g^{S\sigma}\right\rangle\right\rangle & \left\langle\left\langle X_f^{\sigma S} \middle| X_g^{0\sigma}\right\rangle\right\rangle & \left\langle\left\langle X_f^{\sigma S} \middle| X_g^{\bar{\sigma}S}\right\rangle\right\rangle \\ \left\langle\left\langle X_f^{\sigma 0} \middle| X_g^{\bar{\sigma}0}\right\rangle\right\rangle & \left\langle\left\langle X_f^{\sigma 0} \middle| X_g^{S\sigma}\right\rangle\right\rangle & \left\langle\left\langle X_f^{\sigma 0} \middle| X_g^{0\sigma}\right\rangle\right\rangle & \left\langle\left\langle X_f^{\sigma 0} \middle| X_g^{\bar{\sigma}S}\right\rangle\right\rangle \\ \left\langle\left\langle X_f^{S\bar{\sigma}} \middle| X_g^{\bar{\sigma}0}\right\rangle\right\rangle & \left\langle\left\langle X_f^{S\bar{\sigma}} \middle| X_g^{S\sigma}\right\rangle\right\rangle & \left\langle\left\langle X_f^{S\bar{\sigma}} \middle| X_g^{0\sigma}\right\rangle\right\rangle & \left\langle\left\langle X_f^{S\bar{\sigma}} \middle| X_g^{\bar{\sigma}S}\right\rangle\right\rangle \end{bmatrix}. \tag{2}$$

The general form of the system of equations of motion for the Fourier transform of each component of the matrix Green's function $\hat{D}^{\bar{\sigma}}(f,g)$ is:

$$\omega D^{\bar{\sigma}}_{(pq)(q'p')}(\mathbf{k};\omega) = \delta_{pp'}\delta_{qq'}F(pq) + \Omega(pq)\, D^{\bar{\sigma}}_{(pq)(q'p')}(\mathbf{k};\omega) + L^{pq}_j, \tag{3}$$

where the operators L^{pq}_j include higher-order Green's functions. $\Omega(pq) = \varepsilon_p - \varepsilon_q - \mu$ is the energy of the quasiparticle (pq). $F(pq) = \langle X^{pp}\rangle + \langle X^{qq}\rangle$ is the filling factor. The filling factor $F(pq)$ is the sum of the filling numbers, or occupation numbers, of the initial and final states for the quasiparticle excitation (pq) between these states. The sum of the filling numbers appears in the procedure of projecting complex Green's functions to the basis of the original single-particle Green's functions given in formula (2) by averaging the product of two Hubbard X-operators defined at the same sites of crystal lattice. The filling number of cluster eigenstate $\langle X^{pp}\rangle$ can be calculated self-consistently with the chemical potential and kinematic correlators (Appendix A) from the corresponding Green's function by the spectral theorem. The general scheme for calculating the filling factor and filling numbers with basic formulas is given in [57–59], among other works. In the approach used, the influence of such parameters as doping and temperature on the electronic structure is taken into account using filling numbers. In general, strong electron correlations result in two effects, the splitting of a free electron band onto the lower and upper Hubbard subbands, and the redistribution of the electron spectral weight. For a free electron the spectral weight is always 1, while for the Hubbard subbands it is given by the filling factor.

The system of equations (3) for all components of the matrix Green's function $\hat{D}^{\bar{\sigma}}(\mathbf{k};\omega)$ is decoupled within the generalized mean-field approximation using the projection technique of the Mori-Zwanzig formalism type [56]. In this decoupling method, the operators L^{pq}_j are represented as a sum of the reducible and irreducible parts. The reducible part can be linearized with respect to the X-operators of the Hubbard model basis:

$$L^{0\bar{\sigma}}_j = \sum_{lpq} T^{(0\bar{\sigma})(qp)}_j \mathrm{X}^{(pq)}_l + L^{(0\bar{\sigma})(irr)}_j \to \sum_l \left(T^{(0\bar{\sigma})(\bar{\sigma}0)}_j \mathrm{X}^{(0\bar{\sigma})}_l + T^{(0\bar{\sigma})(S\sigma)}_j \mathrm{X}^{(\sigma S)}_l + \Delta^{(0\bar{\sigma})(0\sigma)}_j \mathrm{X}^{(\sigma 0)}_l + \Delta^{(0\bar{\sigma})(\bar{\sigma}S)}_j \mathrm{X}^{(S\bar{\sigma})}_l \right) + L^{(0\bar{\sigma})(irr)}_j, \tag{4}$$

where $T^{(0\bar{\sigma})(qp)}_j = \langle\{L^{0\bar{\sigma}}_j, X^{qp}_l\}\rangle / \langle\{\mathrm{X}^{pq}_l, X^{qp}_l\}\rangle$, $\Delta^{(0\bar{\sigma})(pq)}_j = \langle\{L^{0\bar{\sigma}}_j, X^{pq}_l\}\rangle / \langle\{\mathrm{X}^{qp}_l, X^{pq}_l\}\rangle$ are the coefficients of linearization. The terms $T^{(pq)(q'p')}_j$ define the self-energy operator, they contain hoppings, kinematic, and spin-spin correlation functions in the generalized mean-field approximation. The terms $\Delta^{\alpha\beta}_{\mathbf{k}}$ are superconducting gap functions. Definitions of the terms $T^{\alpha\beta}_{\mathbf{k}}$ are given in Appendix B. Further, in the generalized mean-field approximation we neglect the irreducible operator $L^{pq(irr)}_j$. The Green's function $\hat{D}^{\bar{\sigma}}(\mathbf{k};\omega)$ is defined by the expression:

$$\hat{D}^{\bar{\sigma}}(\mathbf{k};\omega) = \hat{R}^{-1}(\mathbf{k};\omega)\,\hat{F}, \tag{5}$$

where

$$\hat{R}(\mathbf{k};\omega) = \begin{bmatrix} \omega - \Omega(0\bar{\sigma}) - \bar{T}^{11}_{\mathbf{k}} & -\bar{T}^{12}_{\mathbf{k}} & -\Delta^{11}_{\mathbf{k}} & -\Delta^{12}_{\mathbf{k}} \\ -\bar{T}^{21}_{\mathbf{k}} & \omega - \Omega(S\sigma) - \bar{T}^{22}_{\mathbf{k}} & -\Delta^{21}_{\mathbf{k}} & -\Delta^{22}_{\mathbf{k}} \\ -\Delta^{11*}_{\mathbf{k}} & \Delta^{12*}_{\mathbf{k}} & \omega + \Omega(0\sigma) + T^{11}_{\mathbf{k}} & T^{21}_{\mathbf{k}} \\ \Delta^{21*}_{\mathbf{k}} & -\Delta^{22*}_{\mathbf{k}} & T^{12}_{\mathbf{k}} & \omega + \Omega(\bar{\sigma}S) + T^{22}_{\mathbf{k}} \end{bmatrix} \tag{6}$$

and $\hat{F}$ is the matrix with filling factors of quasiparticle excitations $\{(0\bar{\sigma}), (\sigma S), (\sigma 0), (S\bar{\sigma})\}$ on diagonal

$$\hat{F} = \begin{bmatrix} F(0\sigma) & 0 & 0 & 0 \\ 0 & F(\bar{\sigma}S) & 0 & 0 \\ 0 & 0 & F(\bar{\sigma}0) & 0 \\ 0 & 0 & 0 & F(S\sigma) \end{bmatrix}. \tag{7}$$

The electronic structure in the normal orthorhombic phase was studied within the same approach in [52].

The superconducting gaps for the pairing of quasiparticles inside the conduction band $\Delta^{11}_{\mathbf{k}}$, inside the valence band $\Delta^{22}_{\mathbf{k}}$, and between these bands $\Delta^{12}_{\mathbf{k}}$, $\Delta^{21}_{\mathbf{k}}$ are:

$$\Delta^{11}_{\mathbf{k}} = -\frac{1}{NF(0\sigma)} \sum_{\mathbf{q}} \frac{4}{E_{ct}} \left(\left(t^{12}\right)^2 \right)_{\mathbf{k}-\mathbf{q}} \left\langle X^{\sigma S} X^{\bar{\sigma} S} \right\rangle_{\mathbf{q}}, \tag{8}$$

$$\Delta^{21}_{\mathbf{k}} = \frac{(-1)}{NF(0\sigma)} \sum_{\mathbf{q}} \frac{2\left(\left(t^{11} + \bar{t}^{22}\right) t^{12}\right)_{\mathbf{k}-\mathbf{q}}}{E_{ct}} \left\langle X^{\sigma S} X^{\bar{\sigma} S} \right\rangle_{\mathbf{q}},$$

$$\Delta^{12}_{\mathbf{k}} = \frac{1}{NF(\bar{\sigma}S)} \sum_{\mathbf{q}} \frac{2\left(t^{12}\left(\bar{t}^{11} + t^{22}\right)\right)_{\mathbf{k}-\mathbf{q}}}{E_{ct}} \left\langle X^{\sigma S} X^{\bar{\sigma} S} \right\rangle_{\mathbf{q}},$$

$$\Delta^{22}_{\mathbf{k}} = -\frac{1}{NF(\bar{\sigma}S)} \sum_{\mathbf{q}} \frac{4}{E_{ct}} \left(\left(t^{12}\right)^2 \right)_{\mathbf{k}-\mathbf{q}} \left\langle X^{\sigma S} X^{\bar{\sigma} S} \right\rangle_{\mathbf{q}}.$$

The terms $t^{\alpha\beta}$ are the same intraband and interband hopping integrals as $t(pq,mn)$, but written in a more compact form using the indices 1 and 2; their more detailed description is given in Appendix B. The mechanism of superconducting pairing that was taken into account when deriving Eqs. (8) is an antiferromagnetic superexchange interaction. For hole-doped cuprates, we take into account pairing

only inside the valence band. Therefore, in the rest of this paper, we will talk about the superconducting gap $\Delta^{22}_{\mathbf{k}}$, which we will simply denote as $\Delta_{\mathbf{k}}$. Then the superconducting gap can be written as

$$\Delta_{\mathbf{k}} = -\frac{1}{NF(\bar{\sigma}S)}\sum_{\mathbf{q}}\frac{4}{E_{ct}}t^2_{\mathbf{k}-\mathbf{q}}(\bar{\sigma}0,\sigma S)\left\langle X^{\sigma S}X^{\bar{\sigma}S}\right\rangle_{\mathbf{q}}, \tag{9}$$

where $t^2_{\mathbf{k}-\mathbf{q}}(\bar{\sigma}0,\sigma S)/E_{ct} = J_{\mathbf{k}-\mathbf{q}}$ is the effective exchange interaction similar to the antiferromagnetic superexchange interaction in the $t-J$ model [56,60], $E_{ct} = \Omega(\sigma S) - \Omega(0\bar{\sigma})$ is the charge transfer gap between the dispersionless upper and lower Hubbard bands, which is similar to the effective Hubbard U_{eff}. The anomalous average $\left\langle X^{\sigma S}X^{\bar{\sigma}S}\right\rangle_{\mathbf{q}}$ can be obtained from the Green's function $\left\langle\left\langle X^{\bar{\sigma}S}_{\mathbf{q}} \mid X^{\sigma S}_{\mathbf{q}}\right\rangle\right\rangle$. Since the Green's function $\left\langle\left\langle X^{\bar{\sigma}S}_{\mathbf{q}} \mid X^{\sigma S}_{\mathbf{q}}\right\rangle\right\rangle$ depends on the superconducting gap we obtain the self-consistent equation:

$$\Delta_{\mathbf{k}} = \frac{1}{N}\sum_{\mathbf{q}} J_{\mathbf{k}-\mathbf{q}}\Delta_{\mathbf{q}}A_{\mathbf{q}}, \tag{10}$$

where

$$A_{\mathbf{q}} = \frac{1}{B_{\mathbf{q}}}\left[\frac{\varepsilon^2_{1\mathbf{q}}-\xi^2_{1\mathbf{q}}}{\varepsilon_{1\mathbf{q}}}th\frac{\varepsilon_{1\mathbf{q}}}{2kT} - \frac{\varepsilon^2_{2\mathbf{q}}-\xi^2_{1\mathbf{q}}}{\varepsilon_{2\mathbf{q}}}th\frac{\varepsilon_{2\mathbf{q}}}{2kT}\right], \tag{11}$$

$$B_{\mathbf{q}} = \frac{1}{2}\sqrt{\left(\xi^2_{1\mathbf{q}}+\xi^2_{2\mathbf{q}}+2\bar{T}^{12}_{\mathbf{q}}\bar{T}^{21}_{\mathbf{q}}+\left|\Delta_{\mathbf{q}}\right|^2\right)^2 - 4\left(\left(\xi_{1\mathbf{q}}\xi_{1\mathbf{q}}-\bar{T}^{12}_{\mathbf{q}}\bar{T}^{21}_{\mathbf{q}}\right)^2+\xi^2_{1\mathbf{q}}\left|\Delta_{\mathbf{q}}\right|^2\right)},$$

$\xi_{1\mathbf{q}} = \Omega(0\bar{\sigma}) + \bar{T}^{11}_{\mathbf{q}}$, $\xi_{2\mathbf{q}} = \Omega(\sigma S) + \bar{T}^{22}_{\mathbf{q}}$ are the dispersions of quasiparticle excitations inside the conduction (valence) band without interband hybridization in the normal phase, $\pm\varepsilon_{1\mathbf{q}}, \pm\varepsilon_{2\mathbf{q}}$ are the dispersions of the Bogolyubov quasiparticle bands, $\varepsilon_{1\mathbf{q}} = \frac{1}{2}\sqrt{\left(\xi^2_{1\mathbf{q}}+\xi^2_{2\mathbf{q}}+2\bar{T}^{12}_{\mathbf{q}}\bar{T}^{21}_{\mathbf{q}}+\left|\Delta_{\mathbf{q}}\right|^2\right)^2 + B_{\mathbf{q}}}$, $\varepsilon_{2\mathbf{q}} = \frac{1}{2}\sqrt{\left(\xi^2_{1\mathbf{q}}+\xi^2_{2\mathbf{q}}+2\bar{T}^{12}_{\mathbf{q}}\bar{T}^{21}_{\mathbf{q}}+\left|\Delta_{\mathbf{q}}\right|^2\right)^2 - B_{\mathbf{q}}}$. In the orthorhombic phase, the superconducting gap is the sum of d-wave symmetry and extended s^*-wave symmetry: $\Delta_{\mathbf{k}} = \Delta_d\left(\cos(k_x)-\cos\left(k_y\right)\right) + \Delta_{s*}\left(\cos(k_x)+\cos\left(k_y\right)\right)$. Equating the coefficients of the independent functions $\cos(k_x)$ and $\cos\left(k_y\right)$ in the left and right sides of Eq. (10) we obtain the system of equations for linear combinations of the superconducting gap components in the nearest-neighbor hopping approximation:

$$\begin{cases}\Delta_d + \Delta_{s*} = \frac{1}{N}\sum_{\mathbf{q}} 2J^x_{01}A_{\mathbf{q}}\left[\cos^2(q_x)\left(\Delta_d+\Delta_{s*}\right)+\cos(q_x)\cos\left(q_y\right)\left(\Delta_{s*}-\Delta_d\right)\right],\\ \Delta_{s*} - \Delta_d = \frac{1}{N}\sum_{\mathbf{q}} 2J^y_{01}A_{\mathbf{q}}\left[\cos(q_x)\cos\left(q_y\right)\left(\Delta_d+\Delta_{s*}\right)+\cos^2\left(q_y\right)\left(\Delta_{s*}-\Delta_d\right)\right].\end{cases} \tag{12}$$

J^x_{01} and J^y_{01} are the exchange interaction parameters between nearest neighbors along the x and y axis, respectively, $J^x_{01} = 0.168$ eV and $J^y_{01} = 0.164$ eV at the orthorhombic distortion $\delta b/a = 4.15\%$ [52]. The system of Eqs. (12) for the components $\{\Delta_d, \Delta_{s*}\}$ has the form:

$$\Delta_d = \frac{1}{N}\sum_{\mathbf{q}}\Big[A_{\mathbf{q}}\left(J^x_{01}\cos^2(q_x) - \left(J^x_{01}+J^y_{01}\right)\cos(q_x)\cos\left(q_y\right)+J^y_{01}\cos^2\left(q_y\right)\right)\Delta_d + A_{\mathbf{q}}\left(J^x_{01}\cos^2(q_x) + \left(J^x_{01}-J^y_{01}\right)\cos(q_x)\cos\left(q_y\right)-J^y_{01}\cos^2\left(q_y\right)\right)\Delta_{s*}\Big], \tag{13}$$

$$\Delta_{s*} = \frac{1}{N}\sum_{\mathbf{q}}\Big[A_{\mathbf{q}}\left(J^x_{01}\cos^2(q_x) - \left(J^x_{01}-J^y_{01}\right)\cos(q_x)\cos\left(q_y\right)-J^y_{01}\cos^2\left(q_y\right)\right)\Delta_d + A_{\mathbf{q}}\left(J^x_{01}\cos^2(q_x) + \left(J^x_{01}+J^y_{01}\right)\cos(q_x)\cos\left(q_y\right)+J^y_{01}\cos^2\left(q_y\right)\right)\Delta_{s*}\Big]. \tag{14}$$

Introducing the designations

$$D_{1\mathbf{q}} = \frac{A_{\mathbf{q}}}{N}\left(J^x_{01}\cos^2(q_x) - \left(J^x_{01}+J^y_{01}\right)\cos(q_x)\cos\left(q_y\right)+J^y_{01}\cos^2\left(q_y\right)\right), \tag{15}$$

$$D_{2\mathbf{q}} = \frac{A_{\mathbf{q}}}{N}\left(J^x_{01}\cos^2(q_x) + \left(J^x_{01}-J^y_{01}\right)\cos(q_x)\cos\left(q_y\right)-J^y_{01}\cos^2\left(q_y\right)\right),$$

$$S_{1\mathbf{q}} = \frac{A_{\mathbf{q}}}{N}\left(J^x_{01}\cos^2(q_x) - \left(J^x_{01}-J^y_{01}\right)\cos(q_x)\cos\left(q_y\right)-J^y_{01}\cos^2\left(q_y\right)\right),$$

$$S_{2\mathbf{q}} = \frac{A_{\mathbf{q}}}{N}\left(J^x_{01}\cos^2(q_x) + \left(J^x_{01}+J^y_{01}\right)\cos(q_x)\cos\left(q_y\right)+J^y_{01}\cos^2\left(q_y\right)\right)$$

we finally get the expressions for finding of the superconducting gap components:

$$\Delta_d = \sum_{\mathbf{q}}\Delta_{d\mathbf{q}} = \sum_{\mathbf{q}}\left[D_{1\mathbf{q}}\Delta_d + D_{2\mathbf{q}}\Delta_{s*}\right], \tag{16}$$

$$\Delta_{s*} = \sum_{\mathbf{q}}\Delta_{s*\mathbf{q}} = \sum_{\mathbf{q}}\left[S_{1\mathbf{q}}\Delta_d + S_{2\mathbf{q}}\Delta_{s*}\right]. \tag{17}$$

The calculation of the d- and s^*-wave components for each value of temperature and doping is performed using a self-consistent solution of the system of equations (16) and (17) together with the equations for the chemical potential and filling numbers.

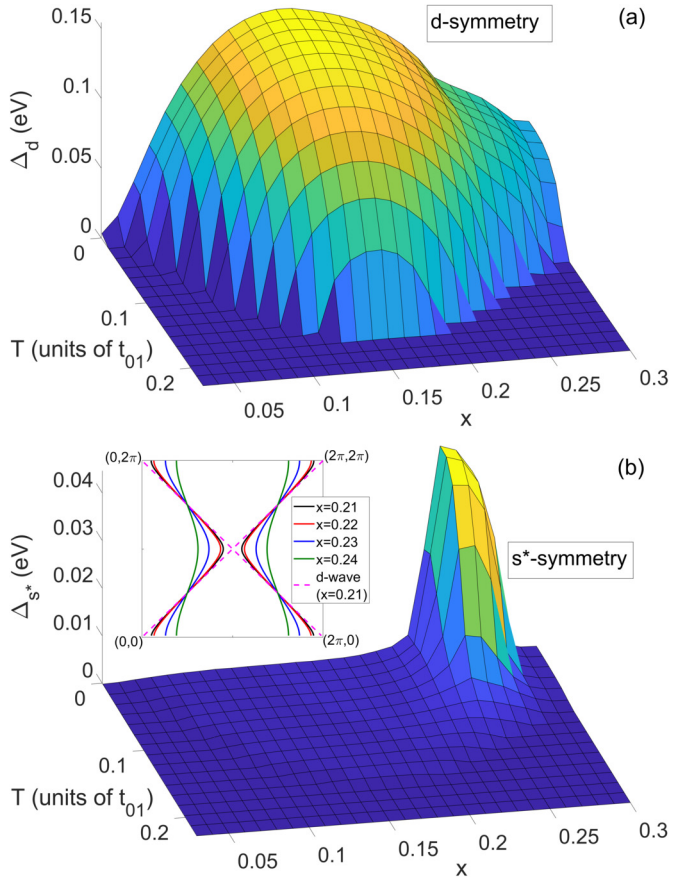

Fig. 1. (Color online) Magnitudes of the superconducting gap components of the (a) d- and (b) extended s^*-wave symmetry in the space of parameters "hole-doping–temperature" (x, T) in the rectangular lattice of CuO_6 octahedra at the orthorhombic distortion $\delta b/a = 4.15\%$. The temperature T is in the units of t_{01} (the interband quasiparticle hopping integral between nearest sites of the crystal lattice along the x axis, $t_{01} = 0.57$ eV). The inset (b) shows the concentration dependence of the lines of the superconducting gap zeros in a system with orthorhombic distortion (solid lines), the purple dotted lines show the nodes of the d-wave superconducting gap.

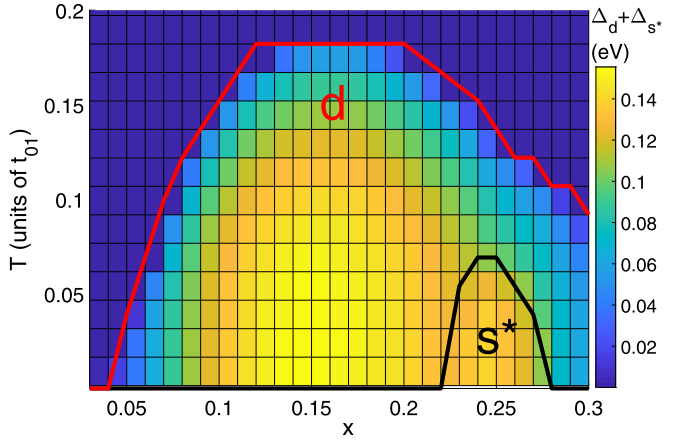

Fig. 2. (Color online) Diagram of the d-wave and s^*-wave symmetry components of the superconducting gap in the space of parameters "hole-doping–temperature" in the rectangular lattice of CuO_6 octahedra which models the HTSC cuprate $La_{2-x}Sr_xCuO_4$. The temperature T is in units of t_{01} (the interband quasiparticle hopping integral between nearest sites of the crystal lattice along the x axis, $t_{01} = 0.57$ eV).

3. Results and discussion

3.1. Concentration and temperature dependences of the d- and extended s*-wave components of the superconducting gap

The concentration and temperature dependence of the d-wave and s^*-wave symmetry components are shown in Fig. 1a, b. The main contribution to the superconducting gap in cuprates comes from the d-wave component. It can be seen from Figs. 1a, b and 2a that the d-wave component prevails over the extended s^*-wave symmetry at all values of doping x and temperature T. The dependence of the d-wave symmetry component on x is different for various T. At $T < 0.1t_{01}$ ($t_{01} \equiv t_{(01)\sigma}$ ($\sigma 0, \bar{\sigma} S$) is the interband quasiparticle hopping integral between the nearest sites of the crystal lattice along the x axis, $t_{01} = 0.57$ eV), the behavior of Δ_d resembles the shape of the

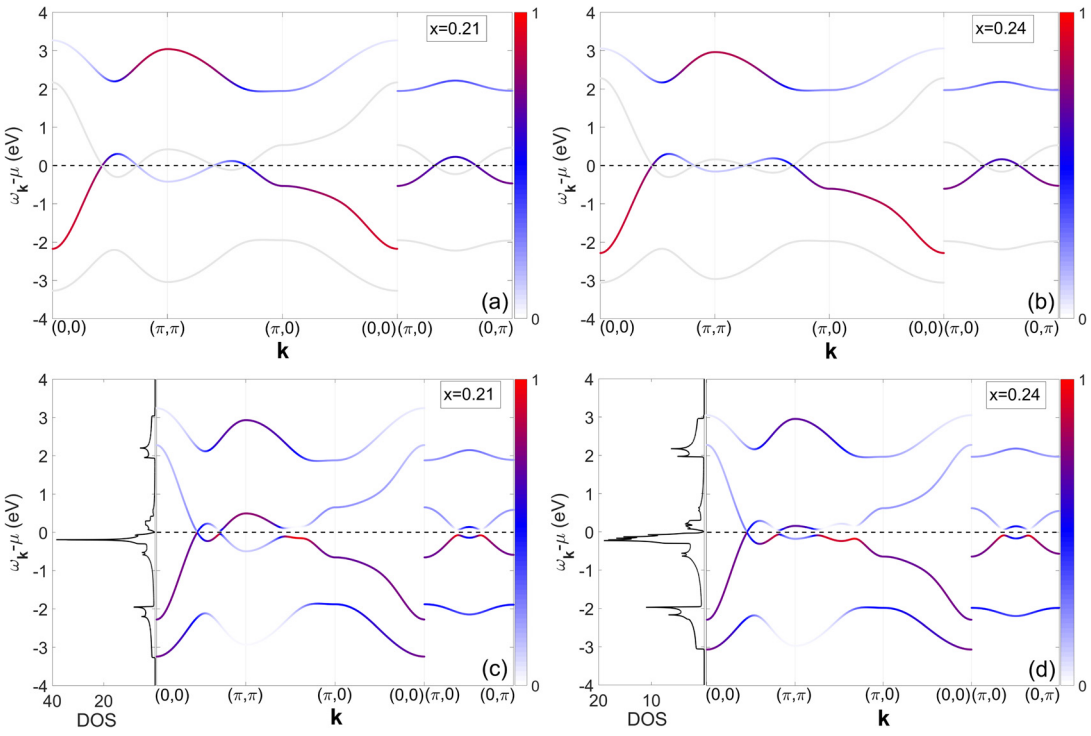

Fig. 3. (Color online) Evolution of the band structure of the quasiparticles in the normal phase (a,b) and Bogolyubov quasiparticles in the superconducting phase (c,d) calculated within the Hubbard model for the rectangular lattice of CuO_6 octahedra with hole doping from $x = 0.21$ to 0.24. The color of each point of the dispersion indicates the spectral weight of the state with the corresponding wave vector **k**. The gray line in (a,b) shows the hole branch of the Bogolyubov quasiparticle band in a system without superconducting pairing. The left panels of (c,d) show the density of states of Bogolyubov quasiparticles in the superconducting phase.

superconducting dome $T_c(x)$ obtained within the Hubbard model for the orthorhombic phase [52]. At $0.1t_{01} < T < 0.19t_{01}$, $\Delta_d(x)$ has a parabolic-like shape with the maximum at $x = 0.14$ (Fig. 1a). An increase in T results in a decrease in $\Delta_d(x)$, the critical temperature at which the superconducting gap closes depends on doping. The contour of the surface $\Delta_d(x, T)$ at $\Delta_d = 0$ forms the concentration dependence of T_c.

The s^*-wave component in the underdoped and optimally doped regimes has a small value, its magnitude is defined by a small value of the orthorhombic distortion. An interesting and unusual property is a sharp increase in the magnitude of the s^*-wave component in the narrow concentration range from $x = 0.22$ to $x = 0.27$ (Fig. 1b), while the d-wave component simply decreases monotonically. The surface $\Delta_{s*}(x, T)$ in this doping range has the shape of a sharp dome (Fig. 1b). An increase in the s^*-wave component in comparison with the d-wave component leads to a significant reconstruction of the lines of zeros of the superconducting gap. The superconducting gap nodes almost coincide with the nodal directions $(0, 0) - (2\pi, 2\pi)$ and $(2\pi, 0) - (0, 2\pi)$ at $x = 0.21$, they bend in such a way that the zero of the superconducting gap at the **k**-point (π, π) disappears (inset of Fig. 1b). The lines of gap zeros in the region of the Brillouin zone center move apart even more with a further increase in x (inset of Fig. 1b). The magnitude of the s^*-wave component decreases with increasing temperature (Fig. 1b). The reduction of the s^*-wave component down to 0 with increasing temperature is more gradual in comparison with a decrease in Δ_d. The maximum of the s^*-wave component at $x = 0.234$ and $T = 0$ K is about half of the d-wave component. It is obvious that a new mechanism of the influence of orthorhombic distortion on the superconducting gap starts to work at overdoping. The location of the region of the enhanced s^*-wave component on the phase diagram (x, T) is depicted in Fig. 2a. The corresponding narrow range of doped hole concentrations is located just behind the pseudogap closing concentration $p^* = 0.22$ in the common phase diagram based on experimental data [61]. In Sections 3.2 and 3.3, we will study in more detail how the transformation of the electronic structure in the doping range from $x = 0.21$ to $x = 0.27$ can change the contributions of various electronic states to the superconducting gap with different symmetry to clarify the reason for the sharp growth of the s^*-wave component.

3.2. Electronic structure of low-energy excitations and its transformation with doping in the overdoped regime

The lower and upper Hubbard electron subbands of cuprates in the normal phase are depicted in Fig. 3a, b (color lines). Two more hole branches (Fig. 3a, b, gray lines) are added when describing the superconducting phase using the Hubbard model in terms of the Gor'kov-Nambu operators in quantum field theory. The bands of Bogolyubov quasiparticles are formed as a result of the mixing of the states of the electron and hole branches due to pairing. A gap equal to the doubled value of the superconducting gap opens between the bands of Bogolyubov quasiparticles. To understand features of the concentration dependence of the superconducting gap, it is necessary to find out what characteristic changes occur in the electronic structure of quasiparticles in the normal phase and Bogolyubov quasiparticles in the superconducting phase with doping. The electronic structure of the $La_{2-x}Sr_xCuO_4$ compound with orthorhombic distortion in the normal phase in a wide doping range was obtained in work [52]. Here we will analyze in more detail the electronic structure of this compound in the normal and superconducting phases in the narrow doping range from $x = 0.21$ to $x = 0.24$, in which there are significant changes in the ratio of the components of the superconducting gap.

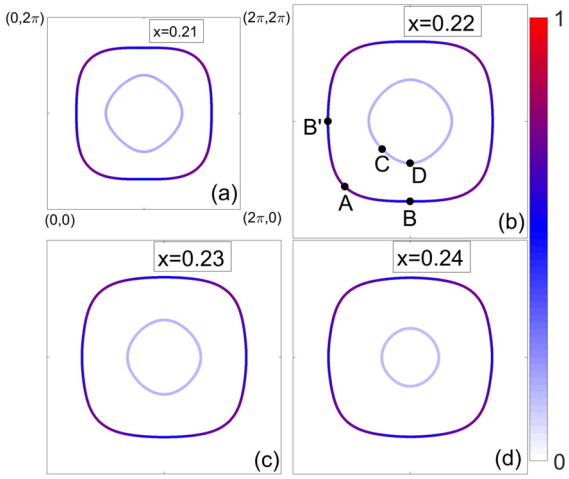

Fig. 4. (Color online) Evolution of the Fermi contours and the superconducting gap nodes with hole doping x calculated within the Hubbard model for the rectangular lattice of CuO_6 octahedra. The Fermi contour is represented by two contours around the point (π, π), the large outer contour consists of the states with a higher spectral weight, the smaller inner electron contour consists of the states with lower intensity.

3.2.1. Reconstruction of the electronic structure with doping in the normal state

First, we will consider the electronic structure in the normal phase, namely the structure of the lower Hubbard band (LHB), since the chemical potential is located inside this band, and the states of this particular band will determine the electronic properties. The LHB in the orthorhombic phase is asymmetric with respect to reflections in the planes passing through the directions $(0, 0) - (2\pi/a, 2\pi/b)$ and $(2\pi/a, 0) - (0, 2\pi/b)$ perpendicular to the $k_x - k_y$ plane [52]. Further in this article, we will be using rescaled values $k'_x = k_x/a$ and $k'_y = k_y/b$, so as not to overload the text with a large number of characters. The LHB has absolute maxima near the points $(\pi/2, \pi/2)$, $(3\pi/2, \pi/2)$, $(\pi/2, 3\pi/2)$, $(3\pi/2, 3\pi/2)$, local maxima at points of the directions $(\pi, 0) - (\pi, 2\pi)$, $(0, \pi) - (2\pi, \pi)$, and a local minimum at the point (π, π) (Fig. 3a, b). The distribution of the spectral weight over the states with different $\mathbf{k}$ is inhomogeneous; the value of the spectral weight is shown in color in Fig. 3a, b. The chemical potential in the doping range from $x = 0.21$ to $x = 0.24$ lies between the local maxima and the local minimum. As a result, a large outer Fermi contour and a small inner electron Fermi contour are formed around the point (π, π) (Fig. 4) [52]. This is precisely the topology of the Fermi contour in the doping range of interest to us. The states of the outer contour have higher spectral intensity in comparison with the states of the inner electron contour. The most significant changes in the band structure with an increase in the hole concentration in the overdoped regime are (i) a decrease in the depth of the inner electron pocket and (ii) the contraction of this pocket. The effect of a decrease in the depth of the small inner pocket is seen when comparing the band structures in Fig. 3a, b. It can be seen that the recess of the dispersion surface around the point (π, π) becomes smaller with a change in doping from $x = 0.21$ to $x = 0.24$. This effect is a consequence of the weakening of spin correlations. An increase in the number of holes results in a shift of the chemical potential deeper into the valence band. The dispersion reconstruction and the shift of the chemical potential caused by doping lead to a decrease in the size of the outer and inner Fermi contours and a change in their shape (Fig. 4a-d). The shape of the outer contour changes insignificantly, as does its size; the contraction of this pocket is maximal in the nodal directions $(0, 0) - (2\pi, 2\pi)$ and $(0, 2\pi) - (2\pi, 0)$, but there is almost no contraction in the antinodal directions $(\pi, 0) - (\pi, 2\pi)$ and $(0, \pi) - (2\pi, \pi)$ (Fig. 4a-d). The shape of the inner contour changes from rectangular with smooth corners at $x = 0.21$ (Fig. 4a) to a circle around the states near $\mathbf{k} = (\pi, \pi)$ at $x = 0.24$ (Fig. 4d). The rate of reduction of the inner Fermi contour upon hole doping is higher than for the outer Fermi contour. The number of states in the inner pocket decreases with hole doping from 12% of the total Brillouin zone at $x = 0.21$ to 0% at $x = 0.28$ (the inner contour disappears, and only the outer contour remains).

3.2.2. Reconstruction of the electronic structure of Bogolyubov quasiparticles with doping in the superconducting state

Let us now consider the electronic structure and its concentration dependence in the superconducting phase. The total dispersion of Bogolyubov quasiparticles for the Hubbard model is shown in Fig. 3c, d. The momentum distribution of the spectral weight of Bogolyubov quasiparticles is inhomogeneous. The upper Hubbard band and its hole branch make a small contribution to the superconducting gap, so it is worth analyzing the two bands formed as a result of hybridization of the lower Hubbard band and its hole branch. These bands are located in the energy range from -2 eV to 2 eV. The dispersion in the energy range below -0.5 eV and above 0.5 eV almost repeats the topology of the lower Hubbard band and its hole branch in the normal state. The bands of Bogolyubov quasiparticles in the energy range determined by 0.5 eV above and below the chemical potential μ are substantially renormalized due to pairing. The spectral functions of Bogolyubov quasiparticles in the region of low-energy excitations along the directions $(0, 0) - (\pi, \pi)$ and $(\pi, \pi) - (\pi, 0)$, as well as their evolution with doping, are shown in Fig. 5. The decrease in the depth of the inner electron pocket around the $\mathbf{k}$-point (π, π) with doping is the most significant change in the electronic structure in the superconducting state as well. It can be seen that the peaks of the spectral functions near the $\mathbf{k}$-point (π, π), corresponding to quasiparticles inside the inner electron pocket, shift closer to the chemical potential as the hole concentration is increased from $x = 0.21$ to $x = 0.27$ (Fig. 5a-c). This effect is more clearly seen in the example of the shift of the peak of the spectral function at the wave vector (π, π) from -0.4 eV to -0.05 eV (Fig. 5d). The increase in the spectral weight of all states inside the inner pocket and, in particular, at the $\mathbf{k}$-point (π, π) with increasing x is also clearly seen (Fig. 5). The jump in the energy of the state at $\mathbf{k} = (\pi, \pi)$ is observed at the concentration $x = 0.234$. This feature indicates a possible relationship between the sharp increase in the s^*-wave component of the superconducting gap and the decrease in the depth of the inner electron pocket, since the maximum of the s^*-wave component is observed at the same concentration $x = 0.234$. The shallowing of the inner electron pocket manifests itself in the density of states as an appearance of additional states near the chemical potential (Fig. 3c, d, left panel).

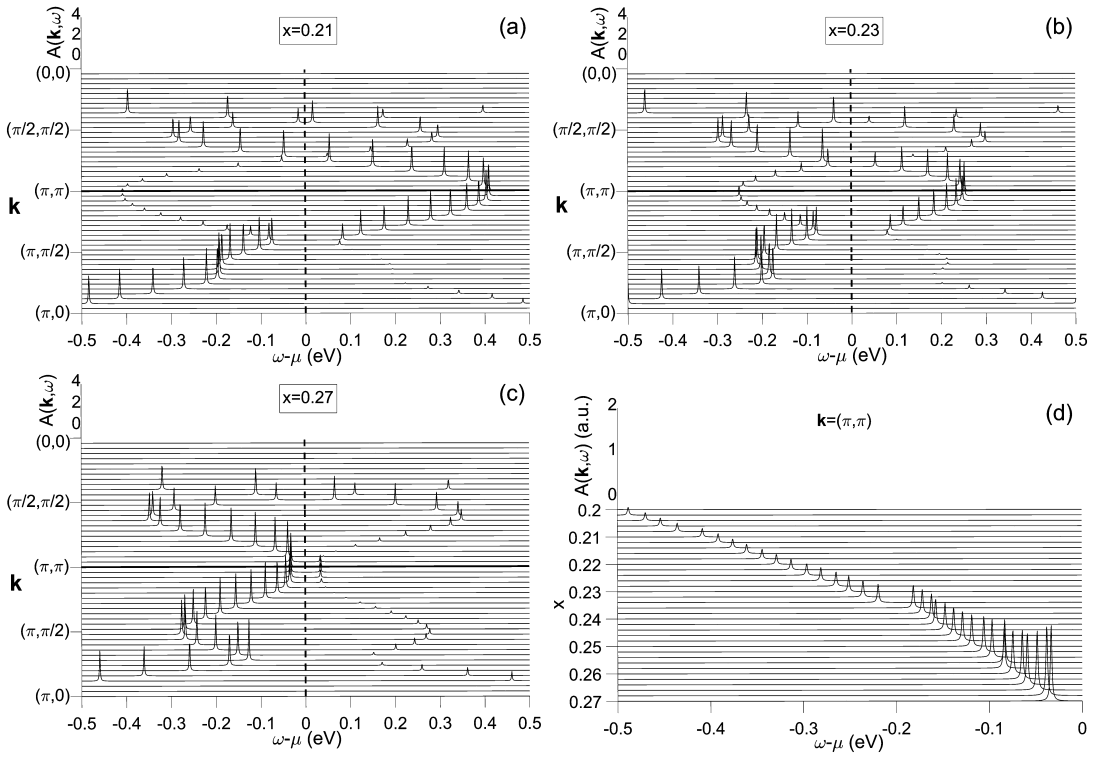

Fig. 5. Spectral functions of Bogolyubov quasiparticles in the region of low-energy excitations along the directions $(0,0)-(\pi,\pi)$ and $(\pi,\pi)-(\pi,0)$ and their concentration dependence. (d) The concentration dependence of the spectral functions at $\mathbf{k}=(\pi,\pi)$ indicating a decrease in the depth of the inner pocket and growth of the spectral weight of states in it with increasing x.

A further increase in the number of doped holes results in an even greater increase in kinematic correlations and a weakening of spin-spin correlations. This raises the energy of electronic excitations with wave vectors in the vicinity of the point (π,π) (Fig. 5c). The points of minimal splitting between two bands of Bogolyubov quasiparticles in the vicinity of (π,π), one of which is visible in the direction $(0,0)-(\pi,\pi)$, the other in the direction $(\pi,\pi)-(\pi,0)$, are shifted towards each other and to the point (π,π) when doping grows. These points under chemical potential form a contour that bounds the small electron pocket, the remaining majority of the original electron pocket is turned inside out. Thus, the electron pocket decreases. At $x=0.27$, it can be seen from the peaks of the spectral functions in the vicinity of the point (π,π) that the bands of the Bogolyubov quasiparticles in this k-region take the form of two almost flat short sections near the chemical potential level (Fig. 5c). A tiny pocket remains in the form of a small pit in this section of the band. When the bands of Bogolyubov quasiparticles approach each other in the vicinity of (π,π), the spectral weight is redistributed from the band above the chemical potential to the band under the chemical potential. Therefore, at $x=0.27$, the peaks of the spectral functions in the band under the chemical potential have high intensity. At $x=0.28$ the pocket disappears, the original pocket in the vicinity of the point (π,π) turns out to be completely inside out. Further, the bands of Bogolyubov quasiparticles begin to repel each other in this region of the Brillouin zone, the dispersion tends to the form characteristic of the band in the strong coupling model with a maximum at the point (π,π).

Although the pairing involves states with all momenta $\mathbf{k}$, the states on the Fermi contours make the largest contribution to the superconducting gap. The $\mathbf{k}$-dependence of the superconducting gap for the states of the Fermi contours is seen from the positions of the BCS spectral function peaks at $\mathbf{k}_F$ when passing from points A and C of the nodal direction to points B and D of the antinodal direction, respectively (Fig. 4b, inset of Fig. 6b). The superconducting gap is close to zero at points A and C (Fig. 6a). The gap at point A of the large outer Fermi contour is smaller than at point C for the smaller inner Fermi contour (Fig. 6a) since point A is closer to the line of zeros of the gap (Fig. 4b, red dashed line) than point C. The latter fact is caused by a stronger deviation of the gap nodes from the nodal direction in the region of $\mathbf{k}$-space in which the inner pocket is located. The superconducting gap at point $A-(0.44\pi,0.44\pi)$ is 0.2 eV larger than its value at point $B-(\pi,0.32\pi)$ (Fig. 6a). A similar increase in the superconducting gap is observed when passing along the inner Fermi contour from the nodal point $C-(0.74\pi,0.74\pi)$ to the antinodal point $D-(\pi,0.6\pi)$ (Fig. 6b), but in this case, the gap increases by only 0.07 eV. Thus superconducting gap for the states of the outer contour is more anisotropic than for the states of the inner contour.

The concentration dependence of the superconducting gap has a different character in different regions of the momentum space. The dependence of the superconducting gap modulus on the Fermi angle Θ (inset of Figs. 7a, b) along the outer Fermi contour at $x=0.21$ and 0.22 (Fig. 7a, black and red lines) can be fit well to a d-wave (Fig. 7a, magenta dotted line) except for slight deviations due to the orthorhombic distortion. The gap decreases over most of the outer contour with increasing doping, while it increases slightly at points near the nodal direction (Figs. 6a, c) since the minimum of the gap moves away from this direction. The deviation of the superconducting gap minimum position from $\Theta=45^\circ$ and the difference in the gap maxima at the points of directions $(0,\pi)-(\pi,\pi)$ $(\Theta=0^\circ)$ and $(\pi,0)-(\pi,\pi)$ $(\Theta=90^\circ)$ become noticeable at $x=0.23$ and $x=0.24$ (Fig. 7a, blue and green lines). A completely different behavior with doping is observed for the profile of the superconducting gap along the inner Fermi contour. The zero of the superconducting gap is significantly displaced from the nodal direction $(0,0)-(\pi,\pi)$ $(\Theta=45^\circ)$ even at $x=0.22$. There is no node of the superconducting gap on the inner contour at $x=0.23$, since the line of gap zeros no longer intersects the contour (Fig. 4c), and therefore the superconducting gap profile differs significantly from the d-wave gap. An even greater deviation of the superconducting gap profile from the d-wave

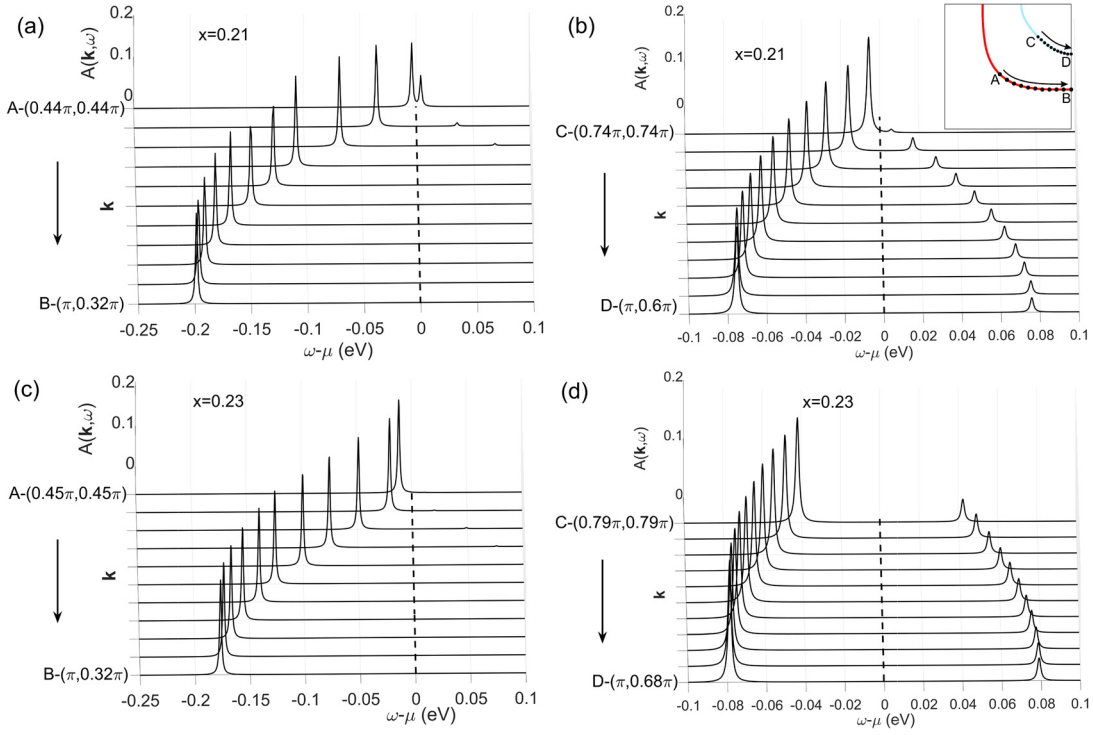

Fig. 6. (Color online) Spectral functions of Bogolyubov quasiparticles at $\mathbf{k}_F$ along the large outer Fermi contour from point A to B (red line in the inset of (b)) and along the small inner Fermi contour from point C to D (blue line in the inset of (b)) and their evolution with hole doping from $x = 0.21$ to $x = 0.23$.

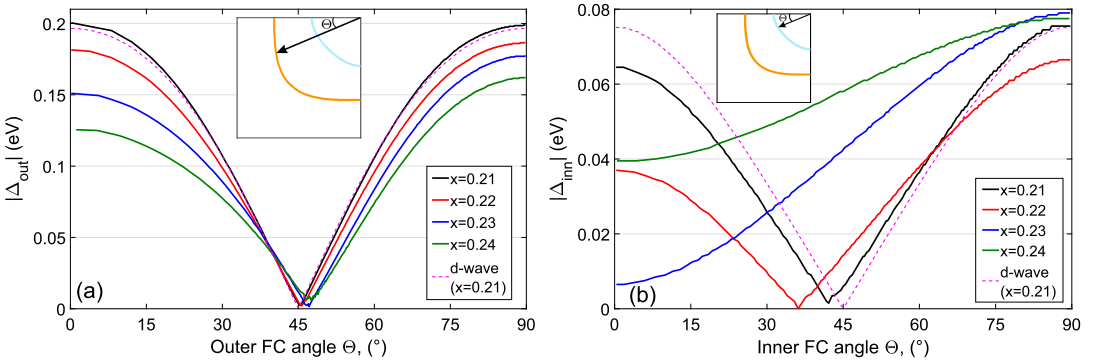

Fig. 7. (Color online) Superconducting gap at $\mathbf{k}_F$ along (a) the outer Fermi contour (orange line in the inset) and (b) the inner Fermi contour (blue line in the inset) as a function of the Fermi angle Θ at different hole doping. The magenta dashed line shows the d-wave gap in the tetragonal phase at $x = 0.21$.

form is observed at $x = 0.23$ and $x = 0.24$: the gap minimum is in the direction $(0, \pi) - (\pi, \pi)$, and the maximum is in the direction $(\pi, 0) - (\pi, \pi)$ (Fig. 7b). A significant increase in the superconducting gap is observed over most of the inner contour; the energy shift of the spectral function peak at the **k**-point C with increasing doping from 0.21 to 0.23 is 0.035 eV (Figs. 6b, d). The spectral function peak at the **k**-point D is hardly shifted with doping.

It can be seen from the spectral functions of the Bogolyubov quasiparticles (Fig. 6) and from the superconducting gap modulus (Fig. 7) that the superconducting gap obtained in our calculations demonstrates the same characteristic properties that are observed in experimental studies of the superconducting gap using ARPES. These characteristic properties are the nodal-antinodal and $a - b$ anisotropies of the superconducting gap, the dependence of the gap on doping, and the anisotropy of the concentration dependence of the gap. It is immediately necessary to clarify that ARPES usually sees one Fermi contour, and this contour corresponds to the outer Fermi contour in our calculations. The absence of inner contour in the ARPES spectra is apparently a consequence of the low spectral intensity of the states of the inner Fermi contour [62]. A significant difference in the intensity of the states of the outer and inner contours can be seen from the difference in their colors in Fig. 4. Since the inner Fermi contour in ARPES is usually not visible, its intensity in real compounds is apparently even lower with respect to the intensity of the states of the outer contour than in the obtained calculations. Thus, to compare the experimental results for the states on the Fermi contour, it is necessary to compare them with the states on the outer Fermi contour in our calculations.

The strong nodal-antinodal anisotropy of the superconducting gap observed in ARPES manifests itself in the fact that the gap is much smaller for the states in the Fermi contour with $\mathbf{k}_F$ in the nodal direction ($\Delta_A^{\text{exp}} = 0.01$ eV, where A is the point of the Fermi contour in the nodal direction) than for states with $\mathbf{k}_F$ in the antinodal direction ($\Delta_B^{\text{exp}} = 0.022$ eV, where B is the point of the Fermi contour in the antinodal direction $(\pi, \pi) - (\pi, 0)$) [29]. The strong anisotropy obtained in our calculations for the states of outer Fermi contour is in

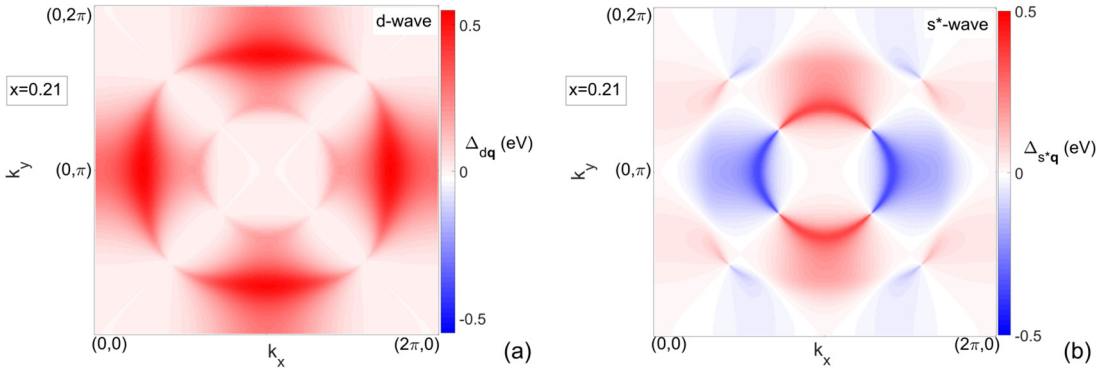

Fig. 8. (Color online) Maps of the partial contributions $\Delta_{d\mathbf{q}}$ (a) and $\Delta_{s*\mathbf{q}}$ (b) of pair states with the wave vector $\mathbf{q}$ to the d-wave and extended s^*-wave components of the superconducting gap, respectively, at hole doping $x = 0.21$. Red (blue) color with different intensity denotes positive (negative) contributions $\Delta_{d\mathbf{q}}$ and $\Delta_{s*\mathbf{q}}$ with different magnitudes.

qualitative agreement with the experimental data, i.e., the gap with $\mathbf{k}_F$ in the antinodal direction Δ_B is much larger than the gap in the nodal direction Δ_A. At x=0.21, the nodal gap $\Delta_A = 0.005$ eV and the antinodal gap $\Delta_B = 0.2$ eV. At x=0.23, $\Delta_A = 0.01$ eV, which even quantitatively coincides with the nodal gap in the ARPES spectra, and $\Delta_B = 0.175$ eV, that is, much more than in ARPES. It can be seen that magnitudes of the nodal gap in our theoretical calculations and in the experimental data are very close. A significant difference is observed in the values of the antinodal gap.

The $a - b$ anisotropy is defined by the difference between the superconducting gaps at the $\mathbf{k}_F$ points of the directions $M - Y$ $((\pi, \pi) - (0, \pi))$ and $M - X$ $((\pi, \pi) - (\pi, 0))$. In the ARPES spectra of overdoped YBCO the superconducting gaps at points Y and X differ by $\Delta_Y^{\text{exp}} - \Delta_X^{\text{exp}} = 0.015$ eV, which is about 50% of the gap [34]. In angle-resolved phase-sensitive measurements in YBCO [63], a 20% larger gap was found along the $M - Y$ direction than along the $M - X$ direction. In our calculations, the difference between the superconducting gaps at the points B' and B (Fig. 4) of the two perpendicular directions can be obtained from Fig. 7, these values at four concentrations are the following: at $x = 0.21$, $\Delta_{B'} - \Delta_B = 0.001$ eV $((\Delta_{B'} - \Delta_B)/\Delta_B = 0.5\%)$; at $x = 0.22$, $\Delta_{B'} - \Delta_B = 0.004$ eV (2%); at $x = 0.23$, $\Delta_{B'} - \Delta_B = 0.024$ eV (16%); at $x = 0.24$, $\Delta_{B'} - \Delta_B = 0.036$ eV (29%). It can be seen from these data that the anisotropy of the superconducting gap on the Fermi contour at points B and B' changes with doping. At $x = 0.23$, the absolute difference between the gaps at points B and B'(24 meV) is close to the experimental value $\Delta_Y^{\text{exp}} - \Delta_X^{\text{exp}}$ (15 meV) [34]. At $x = 0.24$, the difference $\Delta_{B'} - \Delta_B = 0.036$ eV is more than twice the experimental value.

The ARPES spectra for underdoped and overdoped Bi2212 [61] show the dependence of the superconducting gap on doping. The size of the nodal gap remains approximately the same over a wide doping range. The antinodal gap noticeably decreases with increasing doping: from 80 meV for the most weakly doped composition to 50 meV for the most overdoped one. Thus, the dependence of the gap on doping is different for states with $\mathbf{k}_F$ at different points of the Fermi contour. In our calculations, the superconducting gap also decreases with increasing doping for the states of most of the outer Fermi contour, which can be seen from a comparison of the positions of the peaks for different x in Fig. 6 and values of the superconducting gap modulus for different x in Fig. 7a. The gap at point B of the antinodal direction changes by 25 meV as doping increases from $x = 0.21$ to 0.23, i.e. the rate of change is higher than in ARPES measurements, but the trend is correct. The gap at point A of the nodal direction increases by 7 meV as doping increases from $x = 0.21$ to 0.23. The degree of change of the gap in the nodal direction is much weaker, which correlates with the behavior of the nodal gap in ARPES with doping.

The main features of the concentration dependence of the electronic structure are the shallowing of the inner electron pocket around (π, π) and the growth of the spectral weight of states in it. Another important results based on the study of the profile of the superconducting gap along the outer and inner Fermi contours are the difference in the $\mathbf{k}$-dependence of the gap between various regions of the first Brillouin zone and the change in $\mathbf{k}$-dependence with doping. To understand whether there is a relationship between these two effects, it is necessary to analyze the evolution of the partial contributions of pair states with different wave vectors to the superconducting gap as a function of doping.

3.3. Analysis of the momentum-dependent structure of the partial contributions of pair states to the superconducting gap at various doping levels

The structure of the partial contributions of pair states with wave vector $\mathbf{q}$ to the superconducting gap components at various doping levels will be used as a tool for analyzing the concentration dependence of the ratio of these components. The partial contributions of pair states with wave vector $\mathbf{q}$ to the components Δ_d and Δ_{s*} are determined by the terms $\Delta_{d\mathbf{q}}$ of Eq. (16) and $\Delta_{s*\mathbf{q}}$ of Eq. (17), respectively. The surfaces of the contributions $\Delta_{d\mathbf{q}}$ and $\Delta_{s*\mathbf{q}}$ in the first Brillouin zone are shown in Fig. 8. The main contribution to the d-wave component comes from the outer Fermi contour and the states in its vicinity (Fig. 8a), while the contributions $\Delta_{d\mathbf{q}}$ from the states of the inner Fermi contour are much smaller. The main contribution to the s^*-wave component is made by the states of the inner contour (Fig. 8b). It is seen that the contributions $\Delta_{d\mathbf{q}}$ from states with wave vectors over the entire Brillouin zone have the same (positive) sign (Fig. 8a). The contributions to Δ_{s*} from the states with $\mathbf{q}$ along the $(\pi, 0) - (\pi, 2\pi)$ direction have the opposite sign with respect to the contributions $\Delta_{s*\mathbf{q}}$ with $\mathbf{q}$ along the $(0, \pi) - (2\pi, \pi)$ direction (Fig. 8b). The regions of momentum space, in which $\Delta_{s*\mathbf{q}}$ have different signs, are separated by the nodes of the superconducting gap. There is a difference in the size and structure of the $\mathbf{q}$-regions with positive and negative contributions to Δ_{s*}, so Δ_{s*} is nonzero and the s^*-wave component is added to the superconducting gap. As a result, the lines of zeros of the superconducting gap are curves split at point (π, π) (dashed black lines in Fig. 9), and are not straight lines, coinciding with the diagonals of the Brillouin zone, as in the tetragonal phase. The most noticeable uncompensated positive contribution to the s^*-wave component is made by the states with momenta in the vicinity of the $\mathbf{q}$-point (π, π) and along the direction $(\pi, 0) - (\pi, 2\pi)$ between the separated lines of zeros of the superconducting gap (Figs. 9a, b, Figs. 10a, b).

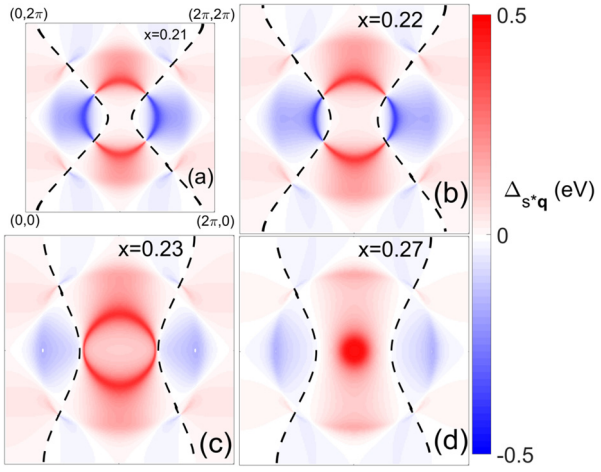

Fig. 9. (Color online) Concentration dependence of the surface of the partial contributions $\Delta_{s*\mathbf{q}}$ of the pair states with wave vectors $\mathbf{q}$ to the extended s^*-wave component of the superconducting gap. Red (blue) color with different intensity denotes positive (negative) contributions $\Delta_{s*\mathbf{q}}$ with different magnitudes. The black dotted lines are the lines of the superconducting gap zeros.

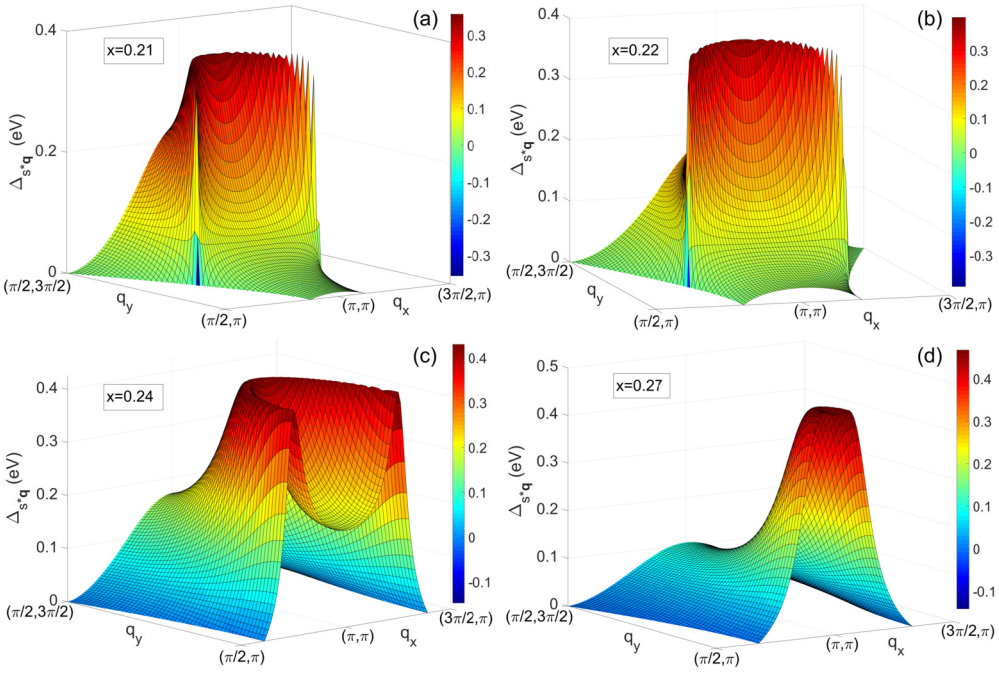

Fig. 10. (Color online) Cuts of the surfaces of the partial contributions $\Delta_{s*\mathbf{q}}$ of the pair states with wave vectors $\mathbf{q}$ to the extended s^*-wave component of the superconducting gap at different hole doping.

We will analyze the concentration dependence of the structure of the contributions $\Delta_{s*\mathbf{q}}$ only from the states of the inner small pocket around (π, π), since these states make the most significant contributions to the s^*-wave component. The analysis shows that there are three mechanisms for the effect of doping on the s^*-wave component, two direct and one indirect. The first mechanism operates over the entire concentration range of doped holes, in which the inner pocket exists: a decrease in the size of the pocket with doping leads to a decrease in the number of contributions, both positive N^+_{iep} and negative N^-_{iep}. The manifestation of this mechanism can be seen in Fig. 11a as a decrease in the total number of contributions N^{tot}_{iep} over the entire range of concentration, a decrease in N^+_{iep} and N^-_{iep} at $x < 0.215$ and N^+_{iep} at $x > 0.234$.

The second mechanism is the most important from the point of view of the formation of the enhanced s^*-wave component. When the doping increases above $x = 0.215$, the depth of the inner electron pocket becomes so small that states of the entire surface of this pocket, and not only on its contour, begin to actively participate in pairing. Further the approach of the energy of states inside the pocket to the level of the chemical potential with doping leads to an increase in the contributions $\Delta_{s*\mathbf{q}}$ from these states (Fig. 10a-d). The total positive contribution Δ^+_{s*} continues to grow up to its maximum at $x = 0.234$ (Fig. 11b). Therefore the maximum of the s^*-wave component is determined by the Δ^+_{s*} maximum. The states inside the inner pocket are involved in the pairing process with s^*-wave symmetry, since they are in the $\mathbf{q}$-region in which the s^*-wave gap with the $\mathbf{q}$-dependence $\cos(q_x) + \cos(q_y)$ has maximum values, and the d-wave gap has minimum values.

Third mechanism is the indirect channel of the influence of the first two mechanisms on the s^*-wave component by the variation of the relative position of the lines of the gap zeros and the inner pocket. This mechanism becomes clear only as part of the procedure for

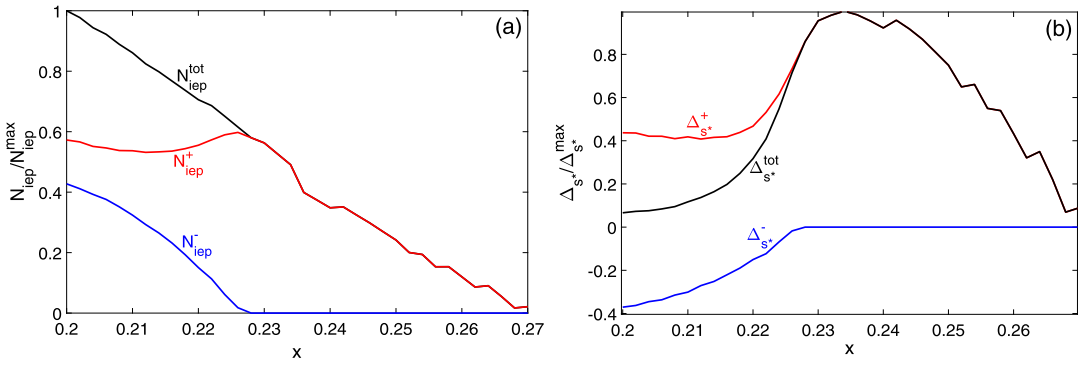

Fig. 11. (Color online) The number of positive N_{iep}^{+} (red line), negative N_{iep}^{-} (blue line), and total contributions N_{iep}^{tot} (black line) of the inner electron pocket states to the s^*-wave superconducting gap at different hole doping. (b) The sum positive contribution Δ_{s*}^{+} (red line), the sum negative contribution Δ_{s*}^{-} (blue line), and total contribution Δ_{s*} (black line) of the inner electron pocket states to the s^*-wave gap.

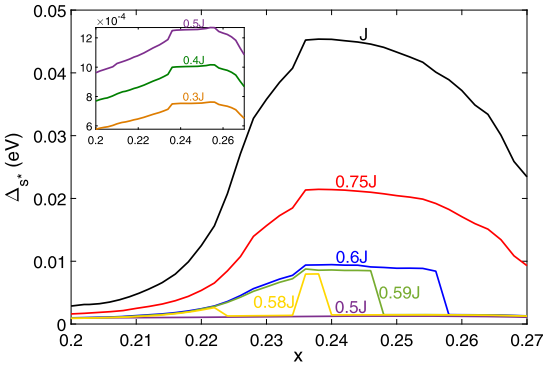

Fig. 12. (Color online) The region of the enhanced s^*-wave component of the superconducting gap upon varying the exchange pairing constant. The variable parameter J' changes from the initial value J (with J_{01}^{x} and J_{01}^{y}) to $0.3J$. The inset demonstrates minor changes in the s^*-wave component at the exchange interaction $J' \leq 0.5J$.

self-consistent determination of the components of the superconducting gap. When the total contributions to the s^*-wave component due to more intense pairing of states inside the pocket exceed the decrease in the total contribution due to the reduction in the area of pocket, the s^*-wave component grows. An increase in the s^*-wave component leads to a transformation of the lines of gap zeros, lines of nodes move away from each other (Fig. 9, dashed black lines). The change in the shape of the gap nodes and the contraction of the inner Fermi contour with doping result in the growth of the positive contributions number N_{iep}^{+} and reduction of the number of negative contributions N_{iep}^{-} (Fig. 9a, b, Fig. 11a, red and blue lines, respectively). At $x = 0.226$, the inner electron pocket is so small that it fits completely into the region between the superconducting gap nodes (Fig. 9c, d), so that all contributions of the inner pocket states $\Delta_{s*\mathbf{q}}$ have a positive sign (Fig. 9c, d; maximum of red line hump in Fig. 11a), and the negative contributions disappear (Fig. 11a, b). Such a mechanism involving the line of the superconducting gap zeros makes the concentration dependence of the s^*-wave component more complex.

3.4. Factors of the s^*-wave component reduction in real compounds

In experimental studies, more modest values of the impurity components of the superconducting gap are usually obtained in comparison with the values that were obtained in our calculations. Raman scattering [64] demonstrates 5% admixture of isotropic s-wave component; thermal conductivity measurements in a rotating magnetic field [10] estimate the maximum admixture component to be 10% of the d-wave component based on the node positions; angle-resolved phase-sensitive measurements also predict 10% value of admixture component [63]. First of all, it should be said that these experimental data do not guarantee that large values of the mixing components will not be found in a certain narrow concentration range, since a thorough systematic study of the superconducting gap for a large number of hole concentrations was not done in these works. However, one can really expect a less significant value of the s^*-wave component. The presence of discrepancies in some characteristics of the electronic structure between our calculations and ARPES data (the absence of the inner Fermi contour in the ARPES data and difference in the values of the antinodal superconducting gap) means that corrections must be taken into account for a realistic description of the superconducting gap. For example, spectral weight of electronic states with wave vectors near (π, π) in real systems can be even weaker than in our calculations, and a weak spectral weight will reduce the contributions of the corresponding pair states to the s^*-wave component.

Large values of the antinodal superconducting gap are obviously associated with a large value of the pairing interaction. The values of the exchange interaction parameters J_{01}^{x} and J_{01}^{y} are close to the values obtained from the experiments on inelastic neutron scattering in cuprates [65] and calculations that take into account the complete basis of quasiparticle cluster excitations [66] ($J = 0.149$ eV). In real compounds, the value of J may be less than that obtained in the calculations. Therefore, it is necessary to investigate how the effect of an increase in the s^*-wave component will change with varying the exchange interaction parameter J. For this, its dependence on doping in the concentration range from 0.21 to 0.27 was calculated with an artificially reduced J (Fig. 12), the reduced parameter J is denoted as J'. The hump of the s^*-wave component gradually subsides as J decreases to 60% of the initial value. The value Δ_{s*} decreases very rapidly

at $J' > 0.6J$ (0.1 eV). The effect of an increase in the s^*-wave component completely disappears at $J' = 0.5J$ (0.08 eV). It is assumed that $J' = 0.5J$ is threshold value of the exchange parameter, at which the involvement of the states in the depth of the shallow electron pocket in the pairing will be extremely weak, analogically to the states in the bands that are far in energy from the chemical potential level. The absence of a large increase in the s^*-wave component in experiments may be due to the fact that the real value of J is less than the threshold value. Another likely scenario is that other pairing mechanisms, such as electron-phonon coupling, in real compounds can compete with the exchange mechanism and may reduce the effects of the latter.

4. Conclusion

In this work, a large magnitude of the extended s^*-wave component of the superconducting gap is found in a narrow doping range in the overdoped HTSC cuprate with orthorhombic distortion, and the reasons for this effect are investigated. The extended s^*-wave symmetry is mixed with the d-wave symmetry due to orthorhombicity, but its fraction is small in the region of weak and optimal doping. In the overdoped regime, the Fermi contour is formed by the large outer and small inner contours around the point (π, π). The states of the inner electron pocket are responsible for the enhanced s^*-wave component since they are located in the region of momentum space, in which the extended s^*-wave superconducting gap has a maximum value and the d-wave gap has a minimum value. Two opposite processes occur with doping. On the one hand, the inner electron pocket decreases, that is, the number of states in this pocket decreases. On the other hand, the pocket becomes shallower, the states in the depth of this pocket become higher in energy and rise to the chemical potential level. The pocket depth becomes so small at a certain concentration of doped holes that states in the depth of the pocket actively participate in pairing. These states make a large contribution to the s^*-wave symmetry gap. The total number of states decreases with further doping, and the total contribution to the s^*-wave component decreases, although the magnitude of the partial contributions in the inner pocket continues to grow. Thus, it turns out that the s^*-wave component fraction under certain conditions depends much more strongly on the electronic structure than on the degree of orthorhombicity. Based on the study, a general conclusion can be drawn regarding the ratio of the several superconducting gap components: the condition for a significant increase in a certain component of the superconducting gap is the presence of shallow and sufficiently large pockets in the region of momentum space in which this component has a significant value, and the competing components have minimum value. The observation of the mixing of the s^*-wave component with the d-wave component precisely in overdoped cuprates can be associated with the presence of certain elements of the electronic structure, such as shallow electron pockets, in the **k**-region of maximum s^*-wave symmetry.

CRediT authorship contribution statement

I.A. Makarov: Writing – original draft, Visualization, Software, Methodology, Investigation, Formal analysis. **S.G. Ovchinnikov:** Writing – review & editing, Validation, Supervision, Resources, Project administration, Methodology, Data curation, Conceptualization.

Declaration of competing interest

The authors declare that they have no known competing financial interests or personal relationships that could have appeared to influence the work reported in this paper.

Acknowledgements

We would like to especially thank A. Bianconi for new ideas, useful discussions, and suggestions. The reported study was funded by Russian Foundation for Basic Research, Government of Krasnoyarsk Territory and Krasnoyarsk Regional Fund of Science according to the research project “Studies of superexchange and electron-phonon interactions in correlated systems as a basis for searching for promising functional materials” No. 20-42-240016.

Appendix A. Filling numbers of local eigenstates

The filling numbers of local eigenstates $\langle X^{pp} \rangle$ are determined self-consistently from the completeness condition $\sum_p X_f^{pp} = 1$, the chemical potential equation:

$$n = 1 + x = 0 \cdot \left\langle X^{0,0} \right\rangle + \sum_\sigma 1 \cdot \langle X^{\sigma\sigma} \rangle + 2 \cdot \left\langle X^{SS} \right\rangle \tag{A.1}$$

(here $n = 1 + x$ is the hole concentration for $La_{2-x}Sr_xCuO_4$) and relation $\langle X^{SS} \rangle = \langle X^{00} \rangle + x$. The filling numbers for zero-, single- and two-hole states $\langle X^{00} \rangle$, $\langle X^{\sigma\sigma} \rangle$, $\langle X^{SS} \rangle$ are defined by the formulas

$$\left\langle X^{00} \right\rangle = \left(-\frac{1}{\pi}\right) \frac{1}{N} \sum_{\mathbf{k}} \int_{-\infty}^{\infty} \frac{1}{\exp\left((\omega - \mu)/kT\right) + 1} \mathrm{Im} \left\langle\left\langle X_{\mathbf{k}}^{0\sigma} \;\middle|\; X_{\mathbf{k}}^{\sigma 0} \right\rangle\right\rangle_{\omega + i\delta} d\omega, \tag{A.2}$$

$$\langle X^{\sigma\sigma} \rangle = \left(-\frac{1}{\pi}\right) \frac{1}{N} \sum_{\mathbf{k}} \int_{-\infty}^{\infty} \frac{1}{\exp\left(-(\omega - \mu)/kT\right) + 1} \mathrm{Im} \left\langle\left\langle X_{\mathbf{k}}^{0\sigma} \;\middle|\; X_{\mathbf{k}}^{\sigma 0} \right\rangle\right\rangle_{\omega + i\delta} d\omega,$$

$$\left\langle X^{SS} \right\rangle = \left(-\frac{1}{\pi}\right) \frac{1}{N} \sum_{\mathbf{k}} \int_{-\infty}^{\infty} \frac{1}{\exp\left(-(\omega - \mu)/kT\right) + 1} \mathrm{Im} \left\langle\left\langle X_{\mathbf{k}}^{\sigma S} \;\middle|\; X_{\mathbf{k}}^{S\sigma} \right\rangle\right\rangle_{\omega + i\delta} d\omega.$$

Note that the filling numbers in zero-hole and two-hole sectors $\langle X^{00}\rangle$ and $\langle X^{SS}\rangle$ are nonzero even in an undoped compound ($x=0$). This fact is caused by the hybridization of quasiparticle excitations between zero- and single-hole states and excitations between single- and two-hole states.

Appendix B. Kinematic parameters

The terms $T_{\mathbf{k}}^{\alpha\beta}$ in the generalized mean-field approximation contain hoppings, kinematic, and spin-spin correlation functions:

$$\bar{T}_{\mathbf{k}}^{11} = F(0\bar{\sigma})\,\bar{t}_{\mathbf{k}}^{11} + \frac{1}{N}\frac{1}{F(0\bar{\sigma})}\sum_{\mathbf{q}}\left(t_{\mathbf{k}-\mathbf{q}}^{11} + \frac{1}{2}\bar{t}_{\mathbf{k}-\mathbf{q}}^{11}\right)C_{\mathbf{q}} + \frac{1}{F(0\bar{\sigma})}a^{11}, \tag{B.1}$$

$$\bar{T}_{\mathbf{k}}^{12} = F(0\bar{\sigma})\,\bar{t}_{\mathbf{k}}^{12} + \frac{1}{N}\frac{1}{F(\sigma S)}\sum_{\mathbf{q}}\left(t_{\mathbf{k}-\mathbf{q}}^{12} - \frac{1}{2}\bar{t}_{\mathbf{k}-\mathbf{q}}^{12}\right)C_{\mathbf{q}} + \frac{1}{F(\sigma S)}a^{12},$$

$$\bar{T}_{\mathbf{k}}^{21} = F(\sigma S)\,\bar{t}_{\mathbf{k}}^{21} + \frac{1}{N}\frac{1}{F(0\bar{\sigma})}\sum_{\mathbf{q}}\left(t_{\mathbf{k}-\mathbf{q}}^{21} - \frac{1}{2}\bar{t}_{\mathbf{k}-\mathbf{q}}^{21}\right)C_{\mathbf{q}} + \frac{1}{F(0\bar{\sigma})}a^{21},$$

$$\bar{T}_{\mathbf{k}}^{22} = F(\sigma S)\,\bar{t}_{\mathbf{k}}^{22} + \frac{1}{N}\frac{1}{F(\sigma S)}\sum_{\mathbf{q}}\left(t_{\mathbf{k}-\mathbf{q}}^{22} + \frac{1}{2}\bar{t}_{\mathbf{k}-\mathbf{q}}^{22}\right)C_{\mathbf{q}} + \frac{1}{F(\sigma S)}a^{22},$$

$$T_{\mathbf{k}}^{11} = F(0\sigma)\,t_{\mathbf{k}}^{11} + \frac{1}{N}\frac{1}{F(0\sigma)}\sum_{\mathbf{q}}\left(\bar{t}_{\mathbf{k}-\mathbf{q}}^{11} + \frac{1}{2}t_{\mathbf{k}-\mathbf{q}}^{11}\right)C_{\mathbf{q}} + \frac{1}{F(0\sigma)}\bar{a}^{11},$$

$$T_{\mathbf{k}}^{12} = F(\bar{\sigma}S)\,t_{\mathbf{k}}^{12} + \frac{1}{N}\frac{1}{F(0\sigma)}\sum_{\mathbf{q}}\left(\bar{t}_{\mathbf{k}-\mathbf{q}}^{12} - \frac{1}{2}t_{\mathbf{k}-\mathbf{q}}^{12}\right)C_{\mathbf{q}} + \frac{1}{F(0\sigma)}\bar{a}^{21},$$

$$T_{\mathbf{k}}^{21} = F(0\sigma)\,t_{\mathbf{k}}^{21} + \frac{1}{N}\frac{1}{F(\bar{\sigma}S)}\sum_{\mathbf{q}}\left(\bar{t}_{\mathbf{k}-\mathbf{q}}^{21} - \frac{1}{2}t_{\mathbf{k}-\mathbf{q}}^{21}\right)C_{\mathbf{q}} + \frac{1}{F(\bar{\sigma}S)}\bar{a}^{12},$$

$$T_{\mathbf{k}}^{22} = F(\bar{\sigma}S)\,t_{\mathbf{k}}^{22} + \frac{1}{N}\frac{1}{F(\bar{\sigma}S)}\sum_{\mathbf{q}}\left(\bar{t}_{\mathbf{k}-\mathbf{q}}^{22} + \frac{1}{2}t_{\mathbf{k}-\mathbf{q}}^{22}\right)C_{\mathbf{q}} + \frac{1}{F(\bar{\sigma}S)}\bar{a}^{22}.$$

In these formulas, $t_{\mathbf{k}}^{\alpha\beta} = \sum_{\lambda\lambda'}\gamma_{\lambda}^{*}(\alpha)\gamma_{\lambda'}(\beta)\,t_{\lambda\lambda'}(\mathbf{k})$ are intra- and interband hoppings of the Hubbard fermions α and β, expressed in terms of the electron hoppings $t_{\lambda\lambda'}(\mathbf{k})$ between the orbitals λ and λ'. The quasiparticle excitation α is defined as a transition between the multielectron CuO_6 cluster eigenstates $|p\rangle$ and $|q\rangle$ with the number of particles differing by one, $\gamma_{\lambda}(\alpha) = \gamma_{\lambda}(pq) = \langle p|\,a_{\lambda}\,|q\rangle$ is the amplitude of such transition, where a_{λ} is the annihilation electron operator on the orbital λ. An explicit form of the hoppings $t_{\mathbf{k}}^{\alpha\beta}$ in the layer of CuO_6 octahedra with orthorhombic distortion is given in [52]. $t_{\mathbf{k}}^{11}$ is the hopping integral of quasiparticles with the spin projection $\sigma = 1/2$ inside the conduction band, $t_{\mathbf{k}}^{22}$ is the hopping integral inside the valence band, $t_{\mathbf{k}}^{12}$, $t_{\mathbf{k}}^{21}$ are the hoppings between the conduction and valence bands. $\bar{t}_{\mathbf{k}}^{11}, \bar{t}_{\mathbf{k}}^{12}, \bar{t}_{\mathbf{k}}^{21}, \bar{t}_{\mathbf{k}}^{22}$ are the same hopping integrals of quasiparticles with the spin projection $\sigma = -1/2$. $C_{\mathbf{q}} = \sum_{fg} C_{fg}e^{i(f-g)\mathbf{q}}$ is the static spin-spin correlation function, $C_{fg} = \left\langle X_f^{\sigma\bar{\sigma}}X_g^{\bar{\sigma}\sigma}\right\rangle$. The values of the spin-spin correlation functions for various hole concentrations were taken from [67]. Terms a^{11}, a^{12}, a^{21}, a^{22}, containing kinematic correlation functions, have the form:

$$a^{11} = \sum_{g}\left(t_{gj}^{22}K_{gj}^{22} - t_{gj}^{11}K_{gj}^{11}\right), \tag{B.2}$$

$$a^{12} = \sum_{g}\left(t_{jg}^{11}K_{jg}^{21} - t_{gj}^{22}K_{gj}^{21} + t_{jg}^{12}K_{jg}^{22} - t_{gj}^{12}K_{gj}^{11}\right),$$

$$a^{21} = \sum_{g}\left(t_{gj}^{11}K_{gj}^{12} - t_{jg}^{22}K_{jg}^{12} + t_{gj}^{21}K_{gj}^{22} - t_{jg}^{21}K_{jg}^{11}\right),$$

$$a^{22} = \sum_{g}\left(t_{jg}^{22}K_{jg}^{22} - t_{gj}^{11}K_{gj}^{11}\right),$$

$$\bar{a}^{11} = \sum_{g}\left(\bar{t}_{jg}^{22}\bar{K}_{jg}^{22} - \bar{t}_{gj}^{11}\bar{K}_{gj}^{11}\right),$$

$$\bar{a}^{12} = \sum_{g}\left(\bar{t}_{gj}^{11}\bar{K}_{gj}^{12} - \bar{t}_{jg}^{22}\bar{K}_{jg}^{12} + \bar{t}_{gj}^{21}\bar{K}_{gj}^{22} - \bar{t}_{jg}^{21}\bar{K}_{jg}^{11}\right),$$

$$\bar{a}^{21} = \sum_{g}\left(\bar{t}_{jg}^{11}\bar{K}_{jg}^{21} - \bar{t}_{gj}^{22}\bar{K}_{gj}^{21} + \bar{t}_{jg}^{12}\bar{K}_{jg}^{22} - \bar{t}_{gj}^{12}\bar{K}_{gj}^{11}\right),$$

$$\bar{a}^{22} = \sum_{g}\left(\bar{t}_{gj}^{22}\bar{K}_{gj}^{22} - \bar{t}_{jg}^{11}\bar{K}_{jg}^{11}\right).$$

The definitions of kinematic correlators are $K_{jg}^{11} = \left\langle X_j^{\sigma 0} X_g^{0\sigma} \right\rangle$, $K_{jg}^{12} = \left\langle X_j^{\sigma 0} X_g^{\bar{\sigma} S} \right\rangle$, $K_{jg}^{21} = \left\langle X_j^{S\bar{\sigma}} X_g^{0\sigma} \right\rangle$, $K_{jg}^{22} = \left\langle X_j^{S\bar{\sigma}} X_g^{\bar{\sigma} S} \right\rangle$, $\bar{K}_{jg}^{11} = \left\langle X_j^{\bar{\sigma} 0} X_g^{0\bar{\sigma}} \right\rangle$, $\bar{K}_{jg}^{12} = \left\langle X_j^{\bar{\sigma} 0} X_g^{\sigma S} \right\rangle$, $\bar{K}_{jg}^{21} = \left\langle X_j^{S\sigma} X_g^{0\bar{\sigma}} \right\rangle$, $\bar{K}_{jg}^{22} = \left\langle X_j^{S\sigma} X_g^{\sigma S} \right\rangle$. The kinematic correlators are calculated self-consistently with the filling numbers of local eigenstates and the chemical potential.

References

[1] K.A. Moler, D.J. Baar, J.S. Urbach, R. Liang, W.N. Hardy, A. Kapitulnik, Magnetic field dependence of the density of states of $YBa_2Cu_3O_{6.95}$ as determined from the specific heat, Phys. Rev. Lett. 73 (1994) 2744–2747, https://doi.org/10.1103/PhysRevLett.73.2744.

[2] K.A. Moler, D.L. Sisson, J.S. Urbach, M.R. Beasley, A. Kapitulnik, D.J. Baar, R. Liang, W.N. Hardy, Specific heat of $YBa_2Cu_3O_{7-\delta}$, Phys. Rev. B 55 (1997) 3954–3965, https://doi.org/10.1103/PhysRevB.55.3954.

[3] N. Momono, M. Ido, T. Nakano, M. Oda, Y. Okajima, K. Yamaya, Low-temperature electronic specific heat of $La_{2-x}Sr_xCuO_4$ and $La_{2-x}Sr_xCu_{1-y}Zn_yO_4$. evidence for a d-wave superconductor, Physica C 723 (1994) 395–401, https://doi.org/10.1016/0921-4534(94)90768-4.

[4] D.A. Wright, J.P. Emerson, B.F. Woodfield, J.E. Gordon, R.A. Fisher, N.E. Phillips, Low-temperature specific heat of $YBa_2Cu_3O_{7-\delta}$, $0 \leq \delta \leq 0.2$: evidence for d-wave pairing, Phys. Rev. Lett. 82 (1999) 1550–1553, https://doi.org/10.1103/PhysRevLett.82.1550.

[5] D.A. Bonn, P. Dosanjh, R. Liang, W.N. Hardy, For rapid suppression of quasiparticle scattering below T_c in $YBa_2Cu_3O_{7-\delta}$, Phys. Rev. Lett. 68 (1992) 2390–2393, https://doi.org/10.1103/PhysRevLett.68.2390.

[6] W.N. Hardy, D.A. Bonn, D.C. Morgan, R. Liang, K. Zhang, Precision measurements of the temperature dependence of λ in $YBa_2Cu_3O_{6.95}$: strong evidence for nodes in the gap function, Phys. Rev. Lett. 70 (1993) 3999–4002, https://doi.org/10.1103/PhysRevLett.70.3999.

[7] D.A. Bonn, W.N. Hardy, Microwave surface impedance of high temperature superconductors, in: D.M. Ginsberg (Ed.), Physical Properties of High-Temperature Superconductors, World Scientific, Singapore, 1996.

[8] M.B. Salamon, F. Yu, V.N. Kopylov, The field dependence of the thermal conductivity: evidence for nodes in the gap, J. Supercond. 8 (1995) 449–452, https://doi.org/10.1007/BF00722827.

[9] F. Yu, M.B. Salamon, A.J. Leggett, W.C. Lee, D.M. Ginsberg, A reply to the comment by R.A. Klemm et al., Phys. Rev. Lett. 77 (1996) 3059, https://doi.org/10.1103/physrevlett.77.3059.

[10] H. Aubin, K. Behnia, M. Ribault, R. Gagnon, L. Taillefer, Angular position of nodes in the superconducting gap of YBCO, Phys. Rev. Lett. 78 (1997) 2624–2627, https://doi.org/10.1103/PhysRevLett.78.2624.

[11] Z.-X. Shen, D.S. Dessau, B.O. Wells, D.M. King, W.E. Spicer, A.J. Arko, D. Marshall, L.W. Lombardo, A. Kapitulnik, P. Dickinson, S. Doniach, J. DiCarlo, T. Loeser, C.H. Park, Anomalously large gap anisotropy in the $a-b$ plane of $Bi_2Sr_2CaCu_2O_{8+\delta}$, Phys. Rev. Lett. 70 (1993) 1553–1556, https://doi.org/10.1103/PhysRevLett.70.1553.

[12] H. Ding, J.C. Campuzano, K. Gofron, C. Gu, R. Liu, B.W. Veal, G. Jennings, Gap anisotropy in $Bi_2Sr_2CaCu_2O_{8+\delta}$ by ultrahigh-resolution angle-resolved photoemission, Phys. Rev. B 50 (1994) 1333–1336, https://doi.org/10.1103/PhysRevB.50.1333.

[13] Z.-X. Shen, D.S. Dessau, Electronic structure and photoemission studies of late transition-metal oxides - *Mott* insulators and high-temperature superconductors, Phys. Rep. 253 (1995) 1–162, https://doi.org/10.1016/0370-1573(95)80001-A.

[14] H. Ding, M.R. Norman, J.C. Campuzano, M. Randeria, A.F. Bellman, T. Yokoya, T. Takahashi, T. Mochiku, K. Kadowaki, Angle-resolved photoemission spectroscopy study of the superconducting gap anisotropy in $Bi_2Sr_2CaCu_2O_{8+x}$, Phys. Rev. B 54 (1996) R9678–R9681, https://doi.org/10.1103/PhysRevB.54.R9678.

[15] D.A. Wollman, D.J.V. Harlingen, W.C. Lee, D.M. Ginsberg, A.J. Leggett, Experimental determination of the superconducting pairing state in YBCO from the phase coherence of YBCO–Pb dc SQUIDs, Phys. Rev. Lett. 71 (1993) 2134–2137, https://doi.org/10.1103/PhysRevLett.71.2134.

[16] D.A. Wollman, D.J.V. Harlingen, J. Giapintzakis, D.M. Ginsberg, Evidence for $d_{x^2-y^2}$ pairing from the magnetic field modulation of $YBa_2Cu_3O_7$–Pb Josephson junctions, Phys. Rev. Lett. 74 (1995) 797–801, https://doi.org/10.1103/PhysRevLett.74.797.

[17] D.A. Brawner, H.R. Ott, Evidence for an unconventional superconducting order parameter in $YBa_2Cu_3O_{6.9}$, Phys. Rev. B 50 (1996) 6530–6533, https://doi.org/10.1103/PhysRevB.50.6530.

[18] D.A. Brawner, H.R. Ott, Evidence for a non-s-wave superconducting order parameter in $YBa_2Cu_3O_{6.6}$ with $T_c = 60$ K, Phys. Rev. B 53 (1996) 8249–8252, https://doi.org/10.1103/PhysRevB.53.8249.

[19] A. Mathai, Y. Gim, R.C. Black, A. Amar, F.C. Wellstood, Experimental proof of a time-reversal-invariant order parameter with a π shift in $YBa_2Cu_3O_{7-\delta}$, Phys. Rev. Lett. 74 (1995) 4523–4527, https://doi.org/10.1103/PhysRevLett.74.4523.

[20] C.C. Tsuei, J.R. Kirtley, C.C. Chi, L.S. Yu-Jahnes, A. Gupta, T. Shaw, J.Z. Sun, M.B. Ketchen, Pairing symmetry and flux quantization in a tricrystal superconducting ring of $YBa_2Cu_3O_{7-\delta}$, Phys. Rev. Lett. 73 (1994) 593–598, https://doi.org/10.1103/PhysRevLett.73.593.

[21] J.R. Kirtley, C.C. Tsuei, J.Z. Sun, C.C. Chi, L.S. Yu-Jahnes, A. Gupta, M. Rupp, M.B. Ketchen, Symmetry of the order parameter in the high-Tc superconductor $YBa_2Cu_3O_{7-\delta}$, Nature 373 (1995) 225–228, https://doi.org/10.1038/373225a0.

[22] C.C. Tsuei, J.R. Kirtley, M. Rupp, J.Z. Sun, A. Gupta, M.B. Ketchen, C.A. Wang, Z.F. Ren, J.H. Wang, M. Bhushan, Pairing symmetry in single-layer tetragonal $Tl_2Ba_2CuO_{6+\delta}$ superconductors, Science 271 (1996) 329–332, https://doi.org/10.1126/science.271.5247.329.

[23] J.R. Kirtley, C.C. Tsuei, H. Raffy, Z.Z. Li, A. Gupta, J.Z. Sun, S. Megtert, Half-integer flux quantum effect in tricrystal $Bi_2Sr_2CaCu_2O_{8+\delta}$, Europhys. Lett. 36 (1996) 707–712, https://doi.org/10.1209/epl/i1996-00291-y.

[24] K.A. Muller, On the macroscopic s- and d-wave symmetry in cuprate superconductors, Philos. Mag. Lett. 82 (2002) 279–288, https://doi.org/10.1080/09500830210131827.

[25] C.C. Tsuei, J.R. Kirtley, Pairing symmetry in cuprate superconductors, Rev. Mod. Phys. 72 (2000) 969–1016, https://doi.org/10.1103/RevModPhys.72.969.

[26] J.F. Annett, N. Goldenfeld, A.J. Leggett, Constraints on the pairing state of the cuprate superconductors, J. Low Temp. Phys. 105 (1996) 473–482, https://doi.org/10.1007/BF00768431.

[27] M. Sigrist, T.M. Rice, Symmetry classification of states in high temperature superconductors, Z. Phys. B 68 (1987) 9–14, https://doi.org/10.1007/BF01307857.

[28] V.P. Mineev, K.V. Samohin, Introduction to Theory of Unconventional Superconductivity, MPhTI, Moscow, 1998.

[29] R.J. Kelley, C. Quitmann, M. Onellion, H. Berger, P. Almeras, G. Margaritondo, Doping-induced change of superconducting gap anisotropy in $Bi_2Sr_2Ca_1Cu_2O_{8+d}$, Science 271 (1996) 1255–1257, https://doi.org/10.1126/science.271.5253.1255.

[30] Guo-meng Zhao, Identification of the bulk pairing symmetry in high-temperature superconductors: evidence for an extended *s* wave with eight line nodes, Phys. Rev. B 64 (2001) 024503, https://doi.org/10.1103/PhysRevB.64.024503.

[31] G. Kotliar, Resonating valence bonds and d-wave superconductivity, Phys. Rev. B 37 (1988) 3664, https://doi.org/10.1103/PhysRevB.37.3664.

[32] Q.P. Li, B.E.C. Koltenbah, R. Joynt, Mixed s-wave and d-wave superconductivity in high-Tc systems, Phys. Rev. B 48 (1993) 437–455, https://doi.org/10.1103/PhysRevB.48.437.

[33] J. Betouras, R. Joynt, Temperature-dependent gap anisotropy in $Bi_2Sr_2CaCu_2O_{8+x}$ as evidence for a mixed-symmetry ground state, Europhys. Lett. 31 (1995) 119–123, https://doi.org/10.1209/0295-5075/31/2/010.

[34] D.H. Lu, D.L. Feng, N.P. Armitage, K.M. Shen, A. Damascelli, C. Kim, F. Ronning, Z.-X. Shen, D.A. Bonn, R. Liang, W.N. Hardy, A.I. Rykov, S. Tajima, Superconducting gap and strong in-plane anisotropy in untwinned $YBa_2Cu_3O_{7-\delta}$, Phys. Rev. Lett. 86 (2001) 4370–4373, https://doi.org/10.1103/PhysRevLett.86.4370.

[35] M.F. Limonov, A.I. Rykov, S. Tajima, A. Yamanaka, Superconductivity-induced effects on phononic and electronic Raman scattering in twin-free $YBa_2Cu_3O_{7-x}$ single crystals, Phys. Rev. B 61 (2000) 12412–12419, https://doi.org/10.1103/PhysRevB.61.12412.

[36] B. Friedl, C. Thomsen, M. Cardona, Determination of the superconducting gap in $RBa_2Cu_3O_{7-\delta}$, Phys. Rev. Lett. 65 (1990) 915–918, https://doi.org/10.1103/PhysRevLett.65.915.

[37] T.P. Devereaux, Theory of electronic Raman scattering in disordered unconventional superconductors, Phys. Rev. Lett. 74 (1995) 4313–4316, https://doi.org/10.1103/PhysRevLett.74.4313.

[38] R.U. Hackl, G. Krug, R. Nemetschek, M. Opel, B. Stadlober, Electronic Raman scattering in copper-oxide superconductors and related compounds, in: Proc. SPIE Spectroscopic Studies of Superconductors, vol. 2696, 1996, pp. 194–204.

[39] T. Strohm, M. Cardona, Determination of the s-wave/d-wave gap ratio in $YBa_2Cu_3O_7$ from electronic Raman scattering and the lmto band structure, Solid State Commun. 104 (1997) 233–236, https://doi.org/10.1016/S0038-1098(97)00267-6.

[40] R. Nemetschek, R. Hackl, M. Opel, R. Philipp, M.T. Béal-Monod, J.B. Bieri, K. Maki, A. Erb, E. Walker, d+s wave superconductivity: analysis of the electronic Raman data of $YBa_2Cu_3O_{7-\delta}$ and other cuprates, Eur. Phys. J. B 5 (1998) 495–503, https://doi.org/10.1007/s100510050471.
[41] T. Masui, M. Limonov, H. Uchiyama, S. Lee, S. Tajima, A. Yamanaka, Raman study of carrier-overdoping effects on the gap in high-Tc superconducting cuprates, Phys. Rev. B 68 (2003), https://doi.org/10.1103/PhysRevB.68.060506, 060506(R).
[42] T. Hiramachi, T. Masui, S. Tajima, Polarization dependence of the electronic Raman spectra of Ca-substituted YBCO single crystals: as a probe of s-wave mixing in the superconducting gap, Physica C 463–465 (2007) 89–92, https://doi.org/10.1016/j.physc.2007.05.009.
[43] N.-C. Yeh, C.-T. Chen, G. Hammerl, J. Mannhart, A. Schmehl, C.W. Schneider, R.R. Schulz, S. Tajima, K. Yoshida, D. Garrigus, M. Strasik, Evidence of doping-dependent pairing symmetry in cuprate superconductors, Phys. Rev. Lett. 87 (2001) 087003, https://doi.org/10.1103/PhysRevLett.87.087003.
[44] A.G. Sun, D.A. Gajewski, M.B. Maple, R.C. Dynes, Observation of Josephson pair tunneling between a high-Tc cuprate ($YBa_2Cu_3O_{7-\delta}$) and a conventional superconductor (Pb), Phys. Rev. Lett. 72 (1994) 2267–2271, https://doi.org/10.1103/PhysRevLett.72.2267.
[45] R. Kleiner, A.S. Katz, A.G. Sun, R. Summer, D.A. Gajewski, S.H. Han, S.I. Woods, E. Dantsker, B. Chen, K. Char, M.B. Maple, R.C. Dynes, J. Clarke, Pair tunneling from c-axis $YBa_2Cu_3O_{7-x}$ to Pb: evidence for s-wave component from microwave induced steps, Phys. Rev. Lett. 76 (1996) 2161–2164, https://doi.org/10.1103/PhysRevLett.76.2161.
[46] K. Zhang, D.A. Bonn, S. Kamal, R. Liang, D.J. Baar, W.N. Hardy, D. Basov, T. Timusk, Measurement of the ab plane anisotropy of microwave surface impedance of untwinned $YBa_2Cu_3O_{6.95}$ single crystals, Phys. Rev. Lett. 73 (1994) 2484–2487, https://doi.org/10.1103/PhysRevLett.73.2484.
[47] D.N. Basov, R. Liang, D.A. Bonn, W.N. Hardy, B. Dabrowski, M. Quijada, D.B. Tanner, J.P. Rice, D.M. Ginsberg, T. Timusk, In-plane anisotropy of the penetration depth in $YBa_2Cu_3O_{7-x}$ and $YBa_2Cu_4O_8$ superconductors, Phys. Rev. Lett. 74 (1995) 598–601, https://doi.org/10.1103/PhysRevLett.74.598.
[48] N.M. Plakida, V.S. Oudovenko, s+d pairing in orthorhombic phase of copper-oxides, Physica C 341 (348) (2000) 289–290, https://doi.org/10.1016/S0921-4534(00)00484-6.
[49] M.V. Eremin, I.A. Larionov, Dispersion of the energy gap in the layered cuprates. Model of the monolayer, JETP Lett. 62 (1995) 192–196.
[50] G. Rohringer, H. Hafermann, A. Toschi, A.A. Katanin, A.E. Antipov, M.I. Katsnelson, A.I. Lichtenstein, A.N. Rubtsov, K. Held, Diagrammatic routes to nonlocal correlations beyond dynamical mean field theory, Rev. Mod. Phys. 90 (2018) 025003, https://doi.org/10.1103/RevModPhys.90.025003.
[51] V. Kresin, S. Ovchinnikov, S. Wolf, Superconducting State: Mechanisms and Materials, Oxford University Press, 2021.
[52] I.A. Makarov, S.G. Ovchinnikov, Effect of orthorhombicity on the electronic structure and superconducting properties of high-Tc cuprate family, J. Supercond. Nov. Magn. 34 (2021) 2503–2515, https://doi.org/10.1007/s10948-021-05915-w.
[53] S.G. Ovchinnikov, I.S. Sandalov, The band structure of strong-correlated electrons in $La_{2-x}Sr_xCuO_4$ and $YBa_2Cu_3O_{7-y}$, Physica C 161 (1989) 607–617, https://doi.org/10.1016/0921-4534(89)90397-3.
[54] V.A. Gavrichkov, S.G. Ovchinnikov, A.A. Borisov, E.G. Goryachev, Evolution of the band structure of quasiparticles with doping in copper oxides on the basis of a generalized tight-binding method, J. Exp. Theor. Phys. 91 (2000) 369–383, https://doi.org/10.1134/1.1311997.
[55] M.M. Korshunov, V.A. Gavrichkov, S.G. Ovchinnikov, I.A. Nekrasov, Z.V. Pchelkina, V.I. Anisimov, Hybrid LDA and generalized tight-binding method for electronic structure calculations of strongly correlated electron systems, Phys. Rev. B 72 (2005) 165104, https://doi.org/10.1103/PhysRevB.72.165104.
[56] N.M. Plakida, L. Anton, S. Adam, G. Adam, Exchange and spin-fluctuation mechanisms of superconductivity in cuprates, J. Exp. Theor. Phys. 97 (2003) 331–342, https://doi.org/10.1134/1.1608998.
[57] S.G. Ovchinnikov, Quasiparticles in strongly correlated electron systems in copper oxides, Phys. Usp. 40 (1997) 993–1017, https://doi.org/10.1070/PU1997v040n10ABEH000289.
[58] S.G. Ovchinnikov, V.V. Val'kov, Hubbard Operators in the Theory of Strongly Correlated Electrons, Imperial College Press, 2004.
[59] M.M. Korshunov, S.G. Ovchinnikov, E.I. Shneyder, V.A. Gavrichkov, Y.S. Orlov, I.A. Nekrasov, Z.V. Pchelkina, Cuprates, manganites, and cobaltites: multielectron approach to the band structure, Mod. Phys. Lett. B 26 (2012) 1230016, https://doi.org/10.1142/S0217984912300165.
[60] P.W. Anderson, Theory of magnetic exchange interactions: exchange in insulators and semiconductors, Solid State Phys. 14 (1963) 99–214, https://doi.org/10.1016/S0081-1947(08)60260-X.
[61] M. Hashimoto, I. Vishik, R.-H. He, T.P. Devereaux, Z.-X. Shen, Energy gaps in high-transition-temperature cuprate superconductors, Nat. Phys. 10 (2014) 483–495, https://doi.org/10.1038/nphys3009.
[62] V.I. Kuz'min, M.A. Visotin, S.V. Nikolaev, S.G. Ovchinnikov, Doping and temperature evolution of pseudogap and spin-spin correlations in the two-dimensional $Hubbard$ model, Phys. Rev. B 101 (2020) 115141, https://doi.org/10.1103/PhysRevB.101.115141.
[63] J.R. Kirtley, C.C. Tsuei, A. Ariando, C.J.M. Verwijs, S. Harkema, H. Hilgenkamp, Angle-resolved phase-sensitive determination of the in-plane gap symmetry in $YBa_2Cu_3O_{7-\delta}$, Nat. Phys. 2 (2006) 190–194, https://doi.org/10.1038/nphys215.
[64] M.F. Limonov, A.I. Rykov, S. Tajima, A. Yamanaka, Raman scattering study on fully oxygenated YBa_2CuO_7 single crystals: x-y anisotropy in the superconductivity-induced effects, Phys. Rev. Lett. 80 (1998) 825–828, https://doi.org/10.1103/PhysRevLett.80.825.
[65] R. Coldea, S.M. Hayden, G. Aeppli, T.G. Perring, C.D. Frost, T.E. Mason, S.W. Cheong, Z. Fisk, Spin waves and electronic interactions in La_2CuO_4, Phys. Rev. Lett. 86 (2001) 5377–5380, https://doi.org/10.1103/PhysRevLett.86.5377.
[66] K.A. Sidorov, V.A. Gavrichkov, S.V. Nikolaev, Z.V. Pchelkina, S.G. Ovchinnikov, Effect of external pressure on the normal and superconducting properties of high-Tc cuprates, Phys. Status Solidi B 253 (2016) 486–493, https://doi.org/10.1002/pssb.201552465.
[67] M.M. Korshunov, S.G. Ovchinnikov, Doping-dependent evolution of low-energy excitations and quantum phase transitions within an effective model for high-Tc copper oxides, Eur. Phys. J. B 57 (2007) 271–278, https://doi.org/10.1140/epjb/e2007-00179-2.